NEURODEGENERATIVE DISEASES

APOE4 exacerbates α-synuclein pathology and related toxicity independent of amyloid

Na Zhao[1], Olivia N. Attrebi[1], Yingxue Ren[2], Wenhui Qiao[1], Berkiye Sonustun[1], Yuka A. Martens[1], Axel D. Meneses[1], Fuyao Li[1], Francis Shue[1,3], Jiaying Zheng[1,3], Alexandra J. Van Ingelgom[1], Mary D. Davis[1], Aishe Kurti[1], Joshua A. Knight[1], Cynthia Linares[1], Yixing Chen[1], Marion Delenclos[1], Chia-Chen Liu[1], John D. Fryer[1,3], Yan W. Asmann[2], Pamela J. McLean[1,3], Dennis W. Dickson[1,3], Owen A. Ross[1,3], Guojun Bu[1,3]*

The apolipoprotein E (*APOE*) ε4 allele is the strongest genetic risk factor for late-onset Alzheimer's disease mainly by driving amyloid-β pathology. Recently, *APOE4* has also been found to be a genetic risk factor for Lewy body dementia (LBD), which includes dementia with Lewy bodies and Parkinson's disease dementia. How *APOE4* drives risk of LBD and whether it has a direct effect on α-synuclein pathology are not clear. Here, we generated a mouse model of synucleinopathy using an adeno-associated virus gene delivery of α-synuclein in human APOE-targeted replacement mice expressing APOE2, APOE3, or APOE4. We found that APOE4, but not APOE2 or APOE3, increased α-synuclein pathology, impaired behavioral performances, worsened neuronal and synaptic loss, and increased astrogliosis at 9 months of age. Transcriptomic profiling in APOE4-expressing α-synuclein mice highlighted altered lipid and energy metabolism and synapse-related pathways. We also observed an effect of *APOE4* on α-synuclein pathology in human postmortem brains with LBD and minimal amyloid pathology. Our data demonstrate a pathogenic role of APOE4 in exacerbating α-synuclein pathology independent of amyloid, providing mechanistic insights into how *APOE4* increases the risk of LBD.

INTRODUCTION

Dementia with Lewy bodies (DLB) is the second most common form of dementia after Alzheimer's disease (AD) (*1*). Dementia also affects about 40% of patients with Parkinson's disease (PD), which is termed PD dementia (PDD) (*2*). These two disorders are collectively referred to as Lewy body dementia (LBD). They differ in timing of cognitive deficits in relation to Parkinsonism, but otherwise, they share many clinical and pathological characteristics, in particular α-synuclein pathology (*3*, *4*). Although the genetic landscape of LBD is incomplete, the most replicated genetic risk factors are at the α-synuclein (*SNCA*) and β-glucocerebrosidase (*GBA*) loci (*5*, *6*) and the ε4 allele of the apolipoprotein E (*APOE4*) gene (*7*–*12*). Because *APOE4* is also the strongest genetic risk factor for late-onset AD, likely by increasing brain amyloid burden (*13*–*15*), which is also found in most patients with LBD, it is difficult to know if *APOE4* contributes to LBD pathogenesis through an amyloid-β (Aβ)–dependent pathway or through other pathways.

LBD is pathologically characterized by neuronal inclusions, Lewy bodies, composed of aggregates of α-synuclein and other proteins (*16*–*18*). In addition to Lewy bodies, the pathology of LBD is also characterized by abnormal accumulation of α-synuclein in neuronal processes, referred to as Lewy neurites. The molecular mechanisms leading to neuronal α-synuclein accumulation and neurodegeneration remain unresolved. A pathogenic role for α-synuclein is supported by the genetic evidence that both point mutations and genomic multiplications (duplications and triplications) of the α-synuclein gene (*SNCA*) cause autosomal dominant familial forms of the LBD (*19*–*23*). Consequently, α-synuclein transgenic mice harboring *SNCA*-A53T or *SNCA*-A30P mutations have been widely used to model LBD, limited by the fact that the mice do not consistently develop neurodegeneration (*24*). Brain overexpression of α-synuclein with adeno-associated virus (AAV) provides an alternative approach to model the disease, in which α-synuclein pathology is accompanied by neurodegeneration (*25*).

To analyze the association of *APOE* genotype on α-synuclein pathology and neurodegeneration in a model system that lacks amyloid, we overexpressed human wild-type α-synuclein using AAV delivery of *SNCA* (*26*, *27*) in mice expressing human APOE2, APOE3, or APOE4 that had been generated by targeted replacement (TR) methods (*28*). We found that APOE4-TR mice overexpressing human α-synuclein (αSyn-APOE4) had conformationally changed and phosphorylated pathogenic α-synuclein, and presented behavioral abnormalities (memory and motor deficits), neuronal loss, synaptic loss, and astrogliosis. These effects were minimal or absent in αSyn-APOE2 and αSyn-APOE3 mice. Transcriptomic profiling of αSyn-APOE4 mice revealed altered lipid and energy metabolism and down-regulated synaptic pathway, which might contribute to the more severe phenotypes in these animals. In human postmortem brains affected by LBD with minimal amyloid pathology, we confirmed that α-synuclein pathology was increased in *APOE4* carriers compared with age- and sex-matched noncarriers.

RESULTS

APOE4 exacerbates α-synuclein pathology in AAV–α-synuclein mouse model

To generate a mouse model of synucleinopathy in the background of different human *APOE* genotypes, we injected AAV–α-synuclein into both lateral ventricles of APOE2-TR, APOE3-TR, and APOE4-TR pups at postnatal day 0 (*27*). High amount of human α-synuclein expression was observed throughout the brain of αSyn-APOE

[1]Department of Neuroscience, Mayo Clinic, Jacksonville, FL 32224, USA. [2]Department of Health Sciences Research, Mayo Clinic, Jacksonville, FL 32224, USA. [3]Neuroscience Graduate Program, Mayo Clinic, Jacksonville, FL 32224, USA.
*Corresponding author. Email: bu.guojun@mayo.edu

mice as demonstrated by immunohistochemistry with an antibody specific to human α-synuclein (fig. S1, A to C). These findings were consistent with previous reports using the same virus (*27*). Control brains injected with AAV–green fluorescent protein (GFP) exhibited GFP expression as expected (fig. S2, A and B) but no detectable human α-synuclein (fig. S1A). There were no differences in the amount of human α-synuclein expression in APOE2-TR, APOE3-TR, or APOE4-TR mice in specific brain regions including cerebral cortex, hippocampus, amygdala, thalamus, striatum, substantia nigra, and cerebellum (fig. S1, A to F). Expression of mRNA for human *SNCA* in cortical regions was confirmed by quantitative polymerase chain reaction (qPCR), and no differences were detected among different APOE isoforms (fig. S3A). There were also no differences in mouse *Snca* mRNA and protein expression in any of the control and α-synuclein–expressing animals (fig. S3, B to D), suggesting that overexpression of human *SNCA* does not affect the expression of mouse endogenous α-synuclein.

To define pathologic α-synuclein in these mice, we performed immunohistochemical staining with an antibody (5G4) that has been previously shown to be specific to conformationally changed pathogenic α-synuclein species in LBD, but not control human postmortem brains (*29*, *30*). We found more 5G4-positive α-synuclein immunoreactivity in αSyn-APOE4 mice compared to αSyn-APOE2 and αSyn-APOE3 mice in the brain regions including the cerebral cortex, hippocampus, amygdala, thalamus, and the overall immunoreactivities in all these brain regions (Fig. 1, A and B). However, we did not observe difference of 5G4-positive α-synuclein immunoreactivity in the region of substantia nigra (fig. S4). Phosphorylation of Ser^{129} of α-synuclein (p-S129) is another characteristic of human synucleinopathies but minimal in normal brains (*31*). Consistently, αSyn-APOE4 mice had more p-S129 immunoreactivity compared to αSyn-APOE2 or αSyn-APOE3 mice in both the cerebral cortex and hippocampus (fig. S5, A to C). The immunoreactivity of p-S129 showed positive correlation with that of 5G4 (fig. S5, D and E), demonstrating the consistency of detecting α-synuclein pathology by these two markers. Collectively, these results suggest that APOE4 selectively exacerbates α-synuclein pathology in a mouse model devoid of amyloid pathology.

To further determine whether the solubility of α-synuclein was affected, we sequentially extracted proteins from half of the brain using reassembly buffer (RAB; representing the nondetergent-soluble fraction), radioimmunoprecipitation assay (RIPA) buffer (representing the detergent-soluble fraction), and SDS lysis buffer (representing the detergent-insoluble fraction). We detected human α-synuclein in all fractions of αSyn-APOE mice by Western blotting (fig. S6A); however, there were no differences in the amount of α-synuclein among APOE isoforms in the three fractions (fig. S6, B to D). We further validated α-synuclein protein expression using an enzyme-linked immunosorbent assay (ELISA) that detects both mouse and human α-synuclein (fig. S7). Total α-synuclein was higher in all fractions of αSyn-APOE mice compared to controls. In contrast, there were no differences in α-synuclein amount with respect to the three APOE isoforms (fig. S7). This suggests that APOE does not affect solubility of α-synuclein at 9 months of age.

APOE4 enhances behavioral deficits in AAV–α-synuclein mice

To determine the effects of APOE isoforms on behavioral performance of αSyn-APOE mice, we evaluated exploration and anxiety-related behaviors, learning and memory performance, as well as motor coordination at 9 months of age. These types of behavior are impaired in human synucleinopathies and have been well characterized in mouse models (*27*, *32*–*34*). In the open-field analysis (OFA), all the APOE-TR mice expressing human α-synuclein displayed a decreased tendency to explore the center of the field (fig. S8A) but did not exhibit hyperactivity as assessed by total distance traveled (fig. S8B) compared to controls. This reflects increased anxiety, which is a common feature of LBD. In the elevated plus maze (EPM) task, αSyn-APOE4 mice spent an increased amount of time in the open arms, whereas αSyn-APOE2 and αSyn-APOE3 mice did not (Fig. 2A), indicating that αSyn-APOE4 mice had aberrant exploratory behavior and disinhibition. In a contextual fear conditioning paradigm, αSyn-APOE4 mice had impairment in auditory cue–associated memory (Fig. 2C), with a trend for impairment in context-associated memory (Fig. 2B). These impairments were not detected in αSyn-APOE2 and αSyn-APOE3 mice, reflecting a memory deficit specific to αSyn-APOE4 mice. Balance and motor coordination were also assessed using hindlimb clasping scores, hangwire tests, and the accelerated rotarod tasks. In all tasks, αSyn-APOE4 mice showed greater deficits. They had higher hindlimb clasping scores (Fig. 2D), decreased latency to fall from the hangwire (Fig. 2E), increased number of falls from the hangwire within 2 min (Fig. 2F), and a decreased latency to fall from the accelerated rotating rod (Fig. 2G) compared to their controls. In contrast to αSyn-APOE4 mice, αSyn-APOE2 and αSyn-APOE3 mice did not display these changes relative to their controls. To evaluate whether the impaired behavioral performance is related to the α-synuclein pathology in the brain, we performed a correlation analysis between the behavioral parameters and the 5G4-positive α-synuclein pathologies (total in Fig. 1B). We found a correlation between 5G4-positive α-synuclein and behavioral performances, such as the EPM, the fear conditioning tests, the hangwire tests, and the hindlimb clasping tests (fig. S9). Together, our findings show that human α-synuclein expression in the brain of APOE4-TR mice is detrimental to behavior, likely reflecting increased α-synuclein pathology in APOE4-TR mice.

APOE4 induces neuronal and synaptic loss and drives astrogliosis in AAV–α-synuclein mouse model

Postmortem studies have shown a substantial degree of neurodegeneration in LBD (*35*, *36*). To evaluate potential neuronal loss in our AAV mouse models, we performed NeuN nuclei immunostaining. We observed an ~10% neuronal loss in αSyn-APOE4 mice compared with their controls at 9 months of age but no neuronal loss in αSyn-APOE2 and αSyn-APOE3 mice compared with their controls (Fig. 3, A and B). To determine whether there were synaptic abnormalities in αSyn-APOE mice, we evaluated the expression of postsynaptic proteins, including the postsynaptic density protein 95 (PSD95), glutamate receptor subtype 2 (GluR2), the subunit of α-amino-3-hydroxy-5-methyl-4-isoxazolepropionic acid receptor (AMPAR), and the NR2A subunit of *N*-methyl-D-aspartate receptor (NMDAR). The expression of PSD95 (Fig. 3, C and D), GluR2 (Fig. 3, C and E), and NR2A (Fig. 3, C and F) was lower in αSyn-APOE4 mice compared to their controls, but this was not observed in αSyn-APOE2 and αSyn-APOE3 mice. Moreover, the correlation analysis revealed that the NeuN immunoreactivity was associated with the 5G4-positive α-synuclein pathologies (fig. S10A). These results provide evidence for APOE4 isoform-specific neurodegeneration in mice overexpressing human α-synuclein. The considerable neuronal and synaptic loss in the APOE4-TR mice likely results from the more severe α-synuclein

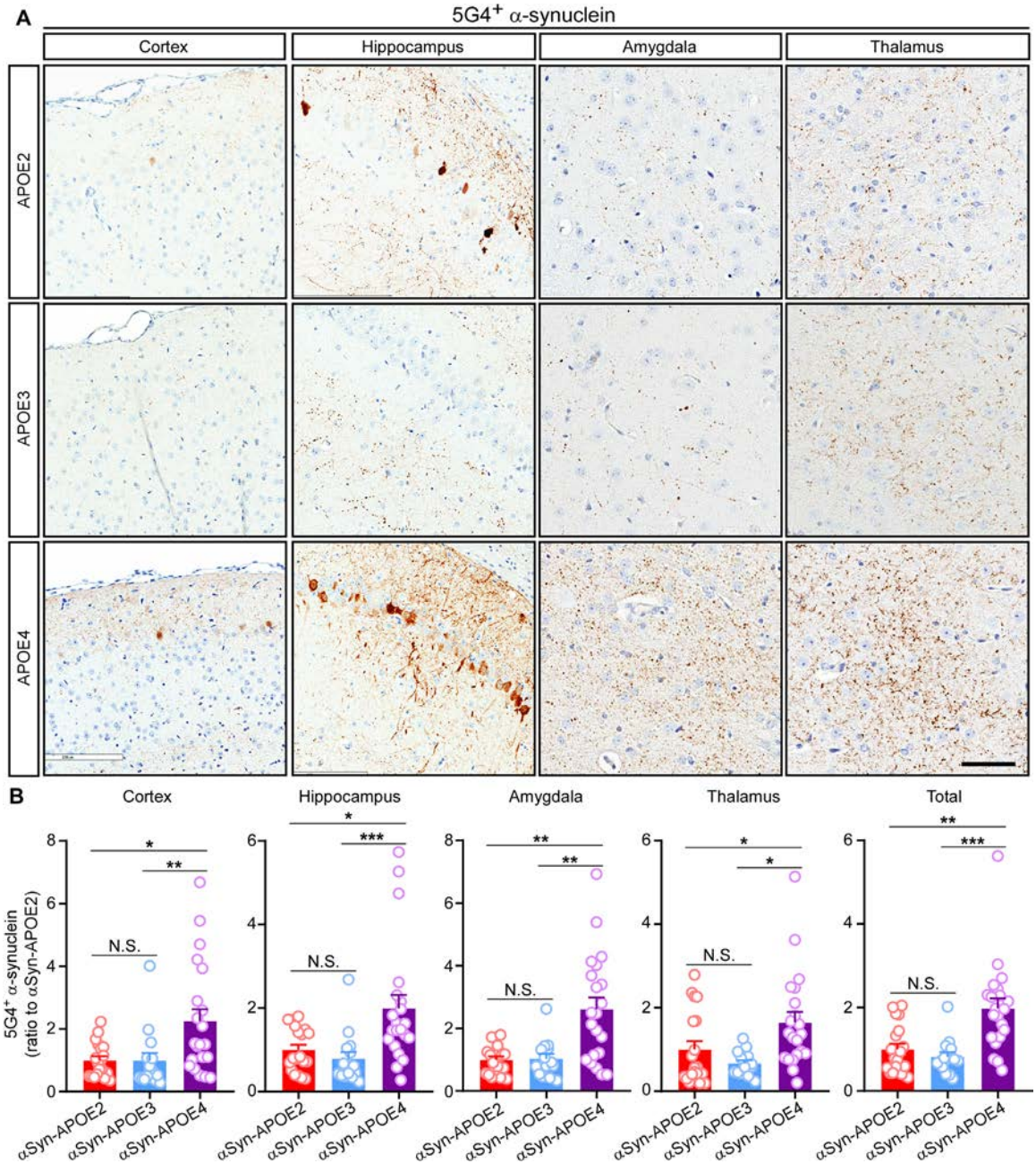

Fig. 1. Increased α-synuclein pathology in αSyn-APOE4 mice. Brain sections were prepared from αSyn-APOE mice at 9 months of age. The conformationally changed pathogenic α-synuclein was determined by immunohistochemical staining with 5G4 antibody. (**A**) Representative images are shown for the deposition of 5G4-positive pathogenic α-synuclein in the brain regions of cerebral cortex, CA1 subfield of the hippocampus, amygdala, and thalamus from αSyn-APOE2, αSyn-APOE3, and αSyn-APOE4 mice. Scale bar, 100 μm. (**B**) The immunoreactivity of 5G4 staining from different brain regions and the overall immunoreactivity from all these regions were evaluated and quantified by Aperio ImageScope ($n = 14$ to 21 mice per group, mixed gender). Data represent means ± SEM relative to the αSyn-APOE2 mice. Kruskal-Wallis tests with Dunn's multiple comparison tests were used. *$P < 0.05$; **$P < 0.01$; ***$P < 0.001$; N.S., not significant.

pathology, which, in turn, might contribute to the enhanced behavioral deficits observed in these mice.

Several lines of evidence indicate that gliosis plays an important role in the neurodegenerative disorders (*37*, *38*). We therefore examined gliosis using an astrocytic marker, glial fibrillary acidic protein (GFAP) (Fig. 4), and microglial marker, ionized calcium-binding adapter molecule 1 (IBA1) (fig. S11). Immunohistochemical staining revealed no difference in GFAP immunoreactivity in all mouse strains (Fig. 4, A and B). However, when we further quantified the expression of *Gfap* mRNA by qPCR and protein by Western blotting, both *Gfap* mRNA (Fig. 4C) and GFAP protein (Fig. 4, D and E) were increased in αSyn-APOE4, but not in αSyn-APOE2 or αSyn-APOE3

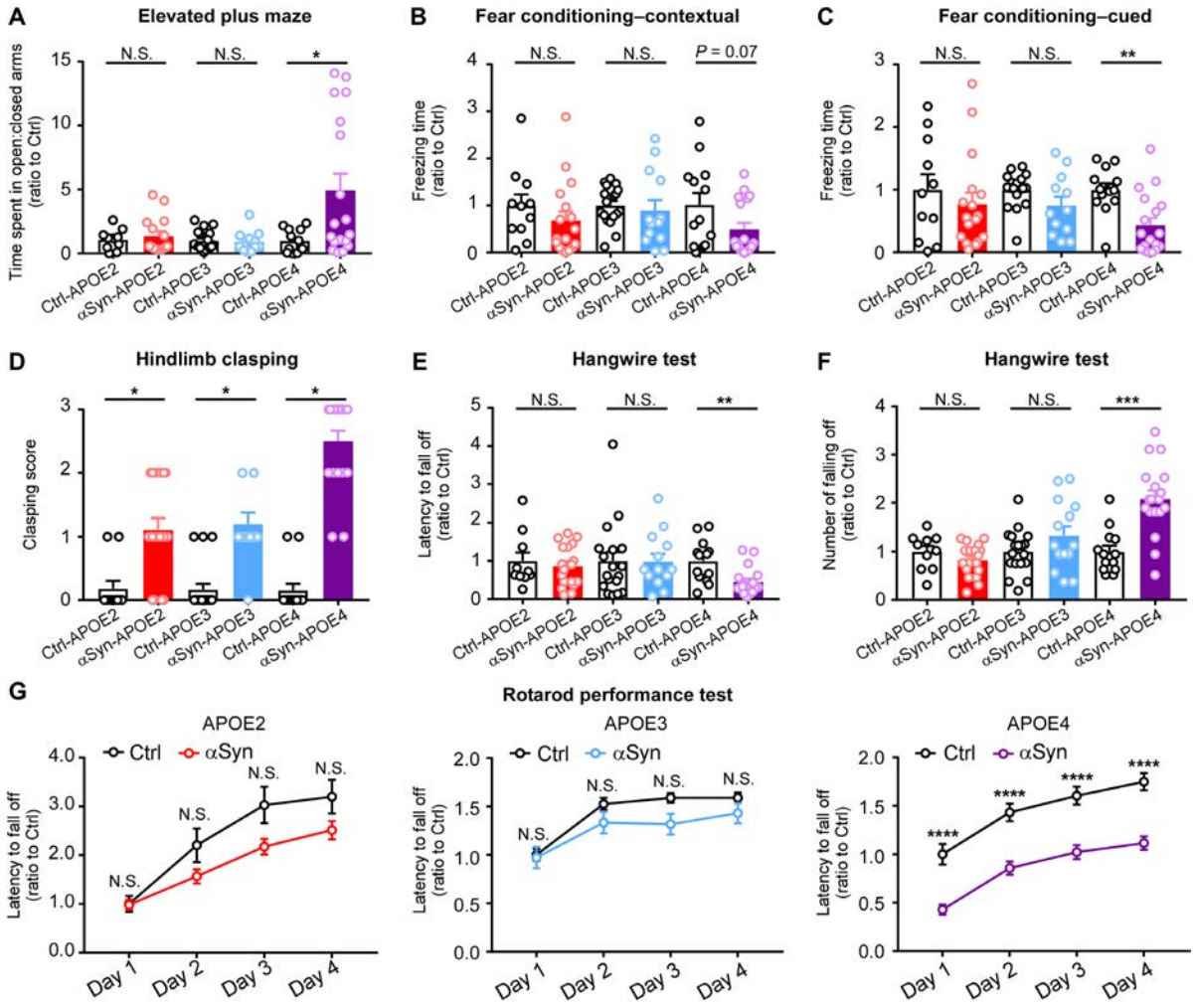

Fig. 2. Impaired behavioral performances in αSyn-APOE4 mice. Behavioral performance was assessed in Ctrl-APOE and αSyn-APOE mice ($n = 10$ to 18 mice per group, mixed gender) at 9 months of age. (**A**) Exploratory behavior was evaluated in the EPM, and the ratios of the time spent in open arms to close arms are shown. (**B** and **C**) Fear conditioning test was used to examine associative memory. The percentage of time with freezing behavior in response to stimulus during contextual and cued tests is shown. (**D**) The hindlimb clasping test was performed to examine the motor coordination. The clasping scores are shown. (**E** and **F**) Hangwire tests were performed to evaluate muscle function and coordination. The latency of the first fall off and numbers of falls within 2 minutes were determined. (**G**) Rotarod performance tests were used to evaluate motor coordination and balance. The latency to fall off was assessed. Data are expressed as means ± SEM relative to their own Ctrl-APOE mice. Mann-Whitney *U* tests followed by Bonferroni correction for multiple comparisons were used. *P* values of <0.0167 were considered statistically significant. *$P < 0.0167$; **$P < 0.01$; ***$P < 0.001$; ****$P < 0.0001$.

mice when compared to their respective controls. Together, these results suggest that human α-synuclein overexpression in APOE4 mice might induce astrogliosis. In contrast to GFAP, IBA1 immunoreactivity was reduced in all the αSyn-APOE mice compared to their controls (fig. S11, A, B, and D), which might be due to the morphological changes of the microglia or a potential toxic effect of α-synuclein on microglia expression of this cell membrane antigen. We next assessed the phagocytic phenotype of these microglia by evaluating CD68 immunohistochemical staining. We found increased CD68 expression in αSyn-APOE4 mice but not in αSyn-APOE2 and αSyn-APOE3 mice (fig. S11, C and E). However, further correlation analysis revealed that neither GFAP nor CD68 immunoreactivity was correlated with 5G4-labeled α-synuclein pathologies (figs. S10B and 11F), suggesting that the activation of astrocyte and microglia in our mouse model might not be directly related to α-synuclein pathology.

APOE4 alters the lipid and energy metabolism and synapse-related pathways in AAV–α-synuclein mouse model identified by transcriptomic profiling

To further evaluate the impact of overexpressing human α-synuclein on the molecular pathogenesis in APOE-TR mice, we performed transcriptomic profiling of cortical samples from the controls (Ctrl-APOE) and αSyn-APOE mice at 9 months of age. We first examined the differentially expressed genes (DEGs) between Ctrl and αSyn mice with respect to *APOE* genotype. We found 79, 57, and 81 DEGs (Benjamini-Hochberg adjusted $P < 0.05$ and $|\text{fold change}| \geq 1.5$) between Ctrl-APOE and αSyn-APOE mice in the background of APOE2-TR, APOE3-TR, or APOE4-TR, respectively (Fig. 5, A to D). An unbiased hierarchical clustering analysis with these DEGs revealed a clear separation between Ctrl and αSyn groups for each *APOE* genotype, reflecting distinct transcriptomic signature changes

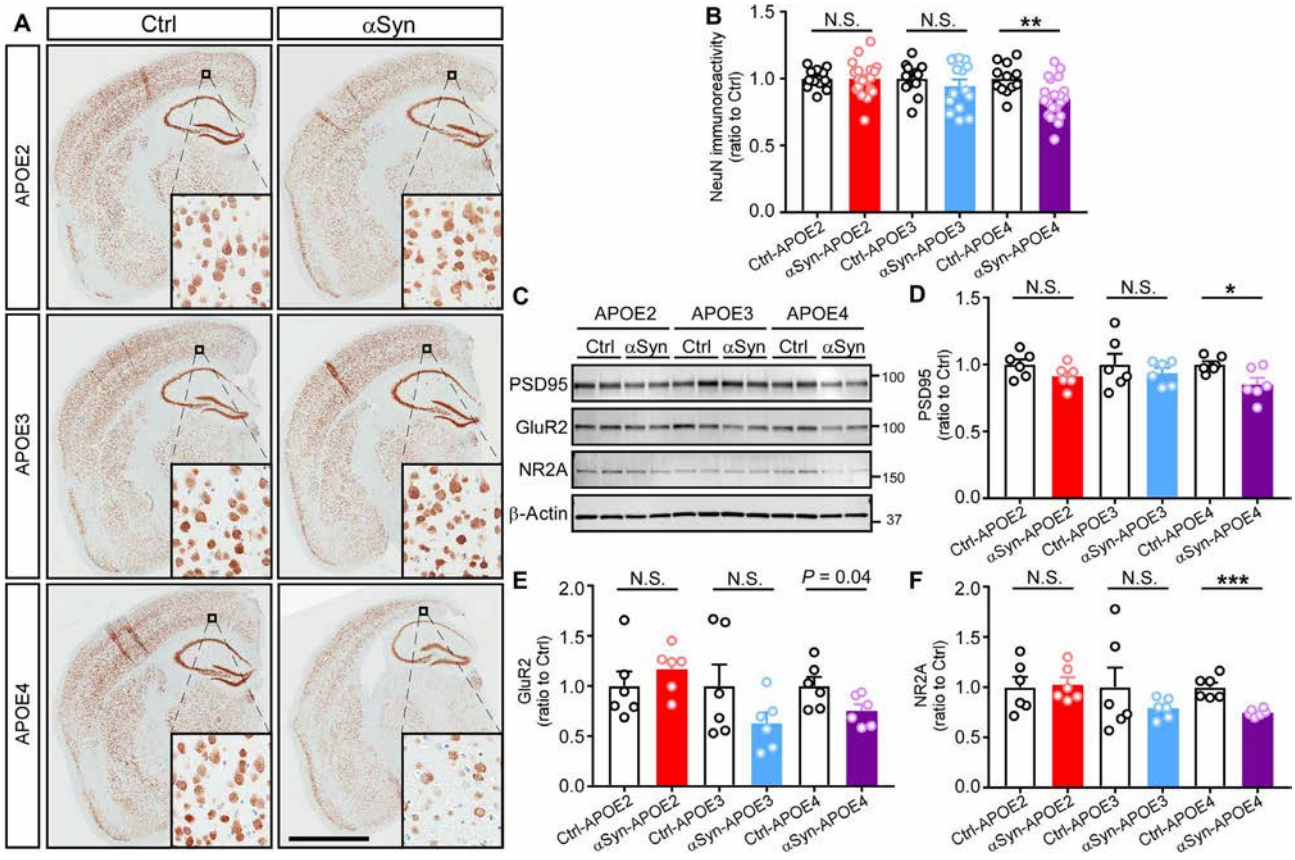

Fig. 3. Neuronal and synaptic loss in αSyn-APOE4 mice. Brain sections and RIPA lysates from Ctrl-APOE and αSyn-APOE mice at 9 months of age were prepared. (**A**) Representative images are shown for the NeuN immunohistochemical staining. Scale bar, 2 mm. (**B**) The immunoreactivity of NeuN staining was evaluated and quantified by Aperio ImageScope ($n = 12$ to 21 mice per group, mixed gender). (**C**) The postsynaptic markers in the cortical RIPA lysate from Ctrl-APOE and αSyn-APOE mice were evaluated by Western blotting at 9 months of age ($n = 6$ mice per group, mixed gender). The amount of PSD95 (**D**), GluR2 (**E**), and NR2A (**F**) was quantified. Results were normalized to β-actin expression. Data represent means ± SEM relative to their own Ctrl-APOE mice. Mann-Whitney *U* tests (B) and Student's *t* tests (D to F) followed by Bonferroni correction for multiple comparisons were used. *P* values of <0.0167 were considered statistically significant. $^*P < 0.0167$; $^{**}P < 0.01$; $^{***}P < 0.001$.

after human α-synuclein expression (fig. S12, A, C, and E). Pathway analyses of DEGs revealed that glycogen synthase activity was the top targeted pathway in APOE4-TR mice (fig. S12F). This pathway was also enriched by DEGs in APOE2-TR mice (fig. S12B), but not in APOE3-TR mice (fig. S12D). These findings suggest that α-synuclein–induced expression differences are affected by *APOE* genotype. We also queried whether there were common DEGs affected by α-synuclein pathology in all three *APOE* genotypes. We found three genes that were differentially expressed in all Ctrl versus αSyn comparisons: *Ak7*, *Spata18*, and *Grp* (Fig. 5E). Expression of these three genes was also validated by qPCR (Fig. 5, H to J).

To further investigate the similarity of α-synuclein–induced gene expression changes in different *APOE* genotype background, we performed transcriptome-wide scatterplots to evaluate potential correlation of gene fold changes of Ctrl versus αSyn in APOE4-TR mice and those of Ctrl versus αSyn in APOE2-TR (Fig. 5F) or APOE3-TR mice (Fig. 5G). Our results showed that the gene fold changes were correlated between APOE4-TR mice and APOE2-TR or APOE3-TR mice after α-synuclein overexpression, indicating a common transcriptomic signature driven by α-synuclein in different *APOE* genotype backgrounds. Because distinct phenotypic changes were only found in αSyn-APOE4 mice, we next explored the specific genes and pathways that were altered by the APOE4-TR mice, but not in APOE2- and APOE3-TR mice after α-synuclein overexpression. We identified a set of genes with different expression amounts between Ctrl and αSyn in APOE4-TR mice, but not in APOE2-TR or APOE3-TR mice (fold change > 1.5; blue dots in Fig. 5, F and G). Subsequently, we performed a pathway enrichment analysis. Regulation of lipid metabolic processes (including phospholipid, ceramide, and sphingolipid) and glycogen synthase activity differed between APOE4 versus APOE2 mice or APOE4 versus APOE3 mice upon α-synuclein overexpression (fig. S13, A and B). The expression of the key genes in each pathway was validated by qPCR, including *Prkcd*, *Apoc1*, *Cry61* (lipid metabolic process, down-regulated in αSyn-APOE4 mice; Fig. 5, K to M), *Igf2* (up-regulated in αSyn-APOE4 mice), and *Ppp1r3g* (glycogen synthase activity pathway, down-regulated in αSyn-APOE4 mice; Fig. 5, N and O).

We identified the molecular networks that were affected by α-synuclein in the brains of APOE4-TR mice using weighted gene coexpression network analyses (WGCNAs) (Fig. 6A). We identified three modules that were dysregulated in Ctrl-APOE4 compared with αSyn-APOE4 mice. These included two down-regulated modules (turquoise and royalblue) and one up-regulated module (blue) in αSyn-APOE4 mice compared to control mice (Fig. 6A). Enrichment analyses revealed impairment of cell communication, as well as

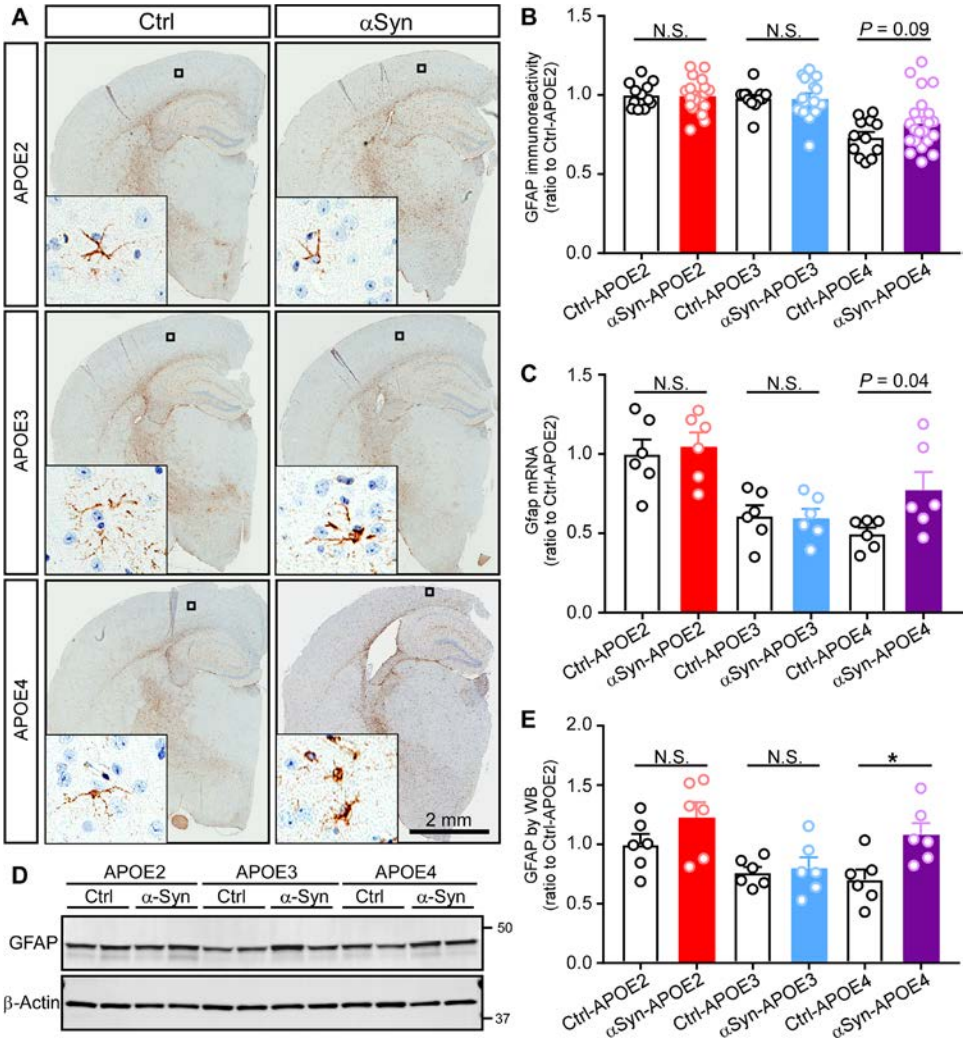

Fig. 4. Astrogliosis in αSyn-APOE4 mice. Brain sections, RNA, and RIPA lysates were prepared from Ctrl-APOE and αSyn-APOE mice at 9 months of age. (**A**) Representative images are shown for the GFAP immunohistochemical staining. Scale bar, 2 mm. (**B**) The immunoreactivity of GFAP staining was evaluated by Aperio ImageScope ($n = 12$ to 21 mice per group, mixed gender). (**C**) The mRNA expression of *Gfap* was determined by qPCR ($n = 6$ mice per group, mixed gender). (**D** and **E**) The GFAP expression in RIPA lysates was assessed by Western blot ($n = 6$ mice per group, mixed gender). The immunoblotting results were normalized to β-actin expression. Data represent means ± SEM relative to Ctrl-APOE2 mice. Mann-Whitney *U* tests (B) and Student's *t* tests (C to E) followed by Bonferroni correction for multiple comparisons were used. *P* values of <0.0167 were considered statistically significant. *$P < 0.0167$.

neuronal and synapse-related pathways in turquoise module genes (Fig. 6, B to D), and protein metabolism and social behavior pathways in royalblue module genes (Fig. 6, E to G). In addition, RNA binding–related pathways were up-regulated in αSyn-APOE4 mice compared to Ctrl-APOE4 mice (Fig. 6, H to J). These results highlight dysregulation of neuronal and synapse-related pathways in αSyn-APOE4 mice, consistent with increased α-synuclein pathology, impaired behavioral performance, and neurodegeneration in these animals.

APOE4 associates with higher amount of α-synuclein pathology in human LBD brains with minimal amyloid pathology

Building on the previous studies by ours (*39*) and other groups (*10*, *40*, *41*), demonstrating that *APOE4* influences the risk of LBD independent of the amounts of AD pathology, we further assessed whether *APOE* genotype influences the severity of α-synuclein pathology in the brains of patients with LBD and minimal amyloid pathology using image analysis of brain sections immunostained for pathological α-synuclein (p-S129 and 5G4). Consistent with findings from mouse models (Fig. 1 and fig. S5), we found higher amount of p-S129 in LBD of *APOE4* carriers compared to those of age- and sex-matched noncarriers (Fig. 7, A and C). The expression of conformationally changed pathogenic α-synuclein detected by 5G4 was not different between carriers and noncarriers (Fig. 7, B and D). The density of 5G4-positive α-synuclein positively correlated with p-S129 burden (Fig. 7E), suggesting a role of phosphorylation in α-synuclein aggregates of patients with LBD. To evaluate whether the glial activation is related to α-synuclein pathology in these human brains, we performed the GFAP and IBA1 immunohistochemical staining. We did not find any difference of GFAP or IBA1 immunoreactivities between *APOE4* carriers and noncarriers (fig. S14, A to D). In addition, there was no correlation between p-S129–positive α-synuclein and GFAP or IBA1 immunoreactivities (fig. S14, E and F), indicating that the glial activation is not associated with α-synuclein pathology in this LBD brain with minimal amyloid pathology, which is consistent with the findings in our mouse models.

DISCUSSION

Although increasingly recognized as a genetic risk factor for LBD, whether and how *APOE4* affects α-synuclein pathology and related toxicity and whether such effects depend on concurrent amyloid pathology are not known. To address this knowledge gap, we used α-synuclein mouse models devoid of amyloid pathology on a background of human APOE2, APOE3, or APOE4. We found overall increased α-synuclein pathology, neurodegeneration, and astrogliosis, as well as behavioral deficits in αSyn-APOE4 mice, which were not present or minimal in αSyn-APOE2 and αSyn-APOE3 mice. Molecular profiling studies revealed several candidate pathways, including lipid and energy metabolism and synaptic pathways, which might contribute to enhanced toxicity of α-synuclein in the setting of APOE4.

APOE4 is the strongest genetic risk factor for late-onset AD, and it has been found to be a consistent genetic risk factor for DLB (*8*–*10*) and PDD (*10*–*12*, *42*). Both DLB and PDD can have concomitant Alzheimer-type pathology (*4*, *43*). In addition, 30 to 40% of individuals

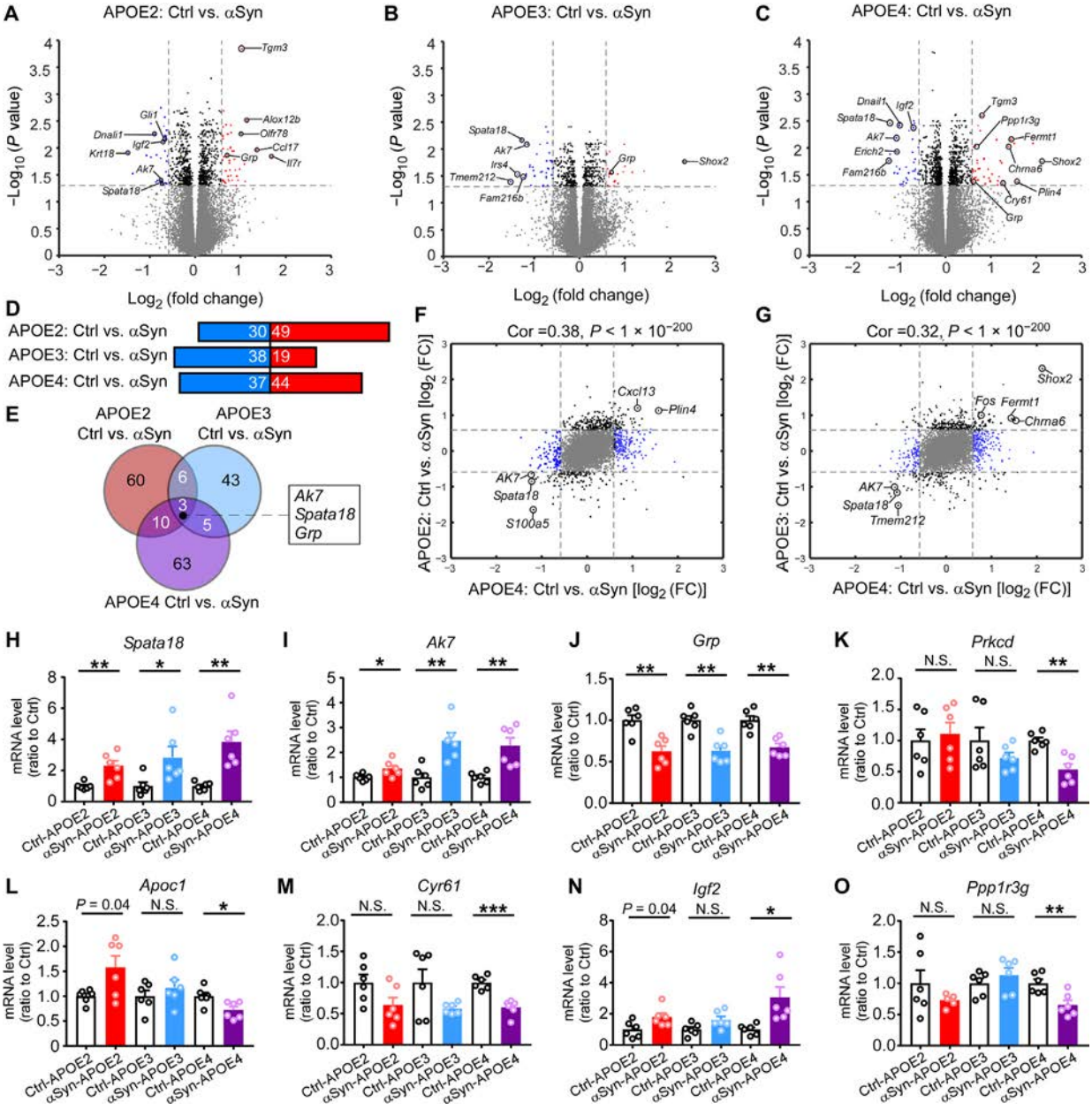

Fig. 5. Transcriptomic profiling of αSyn-APOE mice. RNA sequencing (RNA-seq) was performed using the cortical brain region from Ctrl-APOE and αSyn-APOE mice ($n = 6$ mice per group, mixed gender) at 9 months of age. (**A** to **C**) Volcano plots of differentially expressed genes (DEGs) identified between the Ctrl and αSyn mice in APOE2-TR (A), APOE3-TR (B), and APOE4-TR mice (C) backgrounds. The blue dots denote down-regulated DEGs, and the red dots denote up-regulated DEGs [Benjamini-Hochberg adjusted $P < 0.05$ and |fold change (FC)| ≥ 1.5]. The black circles denote the genes with significant P values (Benjamini-Hochberg adjusted $P < 0.05$), but |fold change| values are less than 1.5, and the gray dots denote the genes without marked differences (Benjamini-Hochberg adjusted $P \geq 0.05$). The gray dotted lines are the reference threshold for P value (0.05) and fold change (±1.5). (**D**) Numbers of DEGs in Ctrl versus αSyn mice are shown. Blue or red bars represent significantly down- or up-regulated genes in each comparison. (**E**) Venn diagram shows the overlapped DEG in Ctrl versus αSyn comparison among APOE2-TR, APOE3-TR, and APOE4-TR mice. (**F** and **G**) Transcriptome-wide scatterplots demonstrate the correlation of fold change in APOE4-TR mice (Ctrl versus αSyn, x axis) and APOE2-TR mice [Ctrl versus αSyn, y axis in (F)], or APOE4-TR mice (Ctrl versus αSyn, x axis) and APOE3-TR mice [Ctrl versus αSyn, y axis in (G)] for all genes (each gene corresponds to one point). The blue dots denote genes changed in APOE4-TR mice but not in APOE2-TR or APOE3-TR mice after α-synuclein overexpression. (**H** to **O**) The key DEGs defined by RNA-seq were validated by qPCR. Data are expressed as means ± SEM relative to their own Ctrl-APOE mice. Student's t tests followed by Bonferroni correction for multiple comparisons were used. P values of <0.0167 were considered statistically significant. *$P < 0.0167$; **$P < 0.01$; ***$P < 0.001$.

with autopsy-confirmed AD also have Lewy bodies (*44*). As such, it is challenging to determine whether *APOE4* contributes to α-synuclein pathology directly or it is dependent on concurrent Aβ pathology. We previously reported that *APOE4* was associated with α-synuclein pathology in LBD cases not only in those with medium or high AD pathology but also in those with low AD pathology (*39*), implying

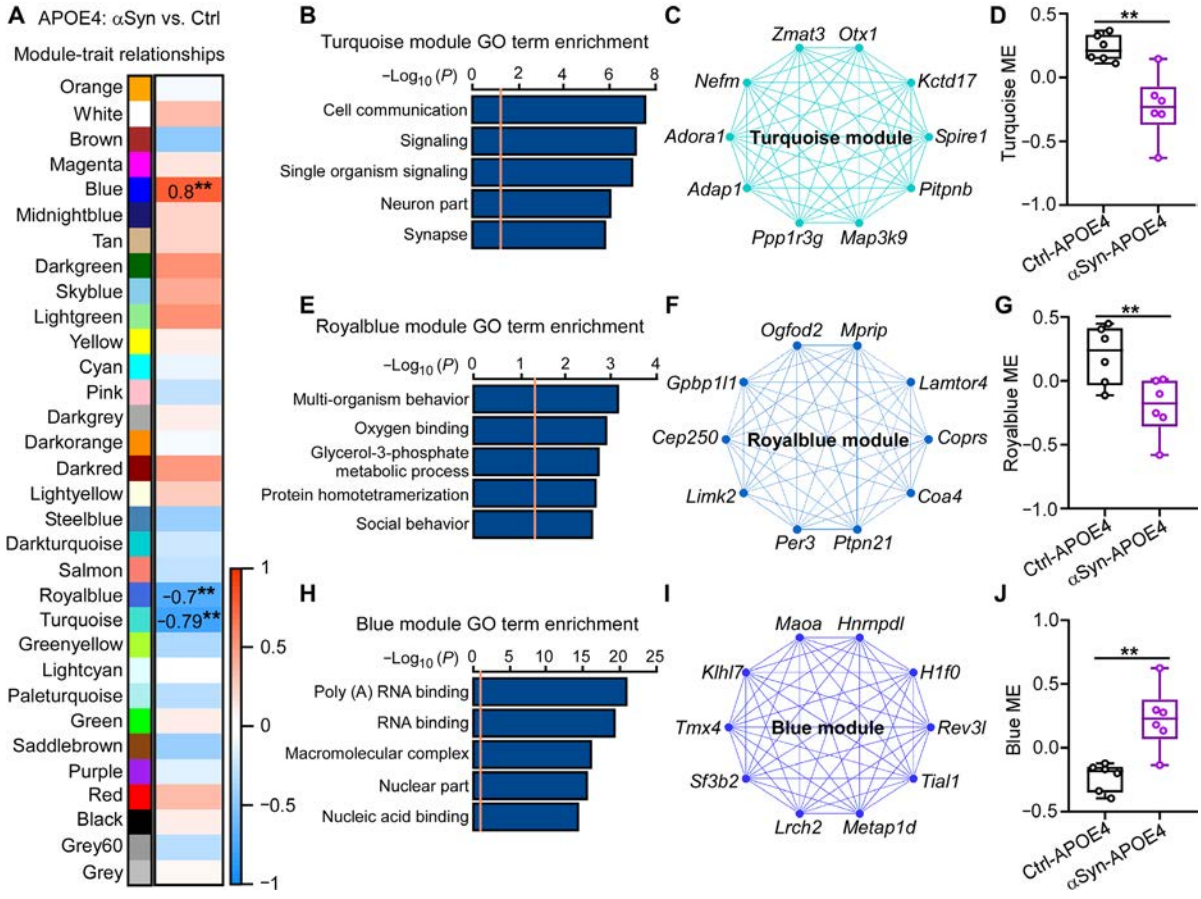

Fig. 6. WGCNA in αSyn-APOE4 mice. (**A**) Modules associated with the comparison of Ctrl versus αSyn in APOE4 mice ($n = 6$ mice per group). Numbers in the heatmap show the correlation coefficient. Modules with positive values (orange) indicate up-regulation in αSyn compared to Ctrl mice; modules with negative values (blue) indicate down-regulation. (**B**) Gene ontology (GO) term enrichment of the turquoise module using 4149 module genes. The orange dotted line indicates the threshold of significance ($P = 0.05$). (**C**) Network plot of the top 10 genes with the highest intramodular connectivity (hub genes) in the turquoise module. (**D**) Trajectory of the module eigengenes (MEs) in the turquoise module between Ctrl-APOE4 and αSyn-APOE4 mice. (**E**) GO term enrichment of the royalblue module using 147 module genes. (**F**) Network plot of the top 10 hub genes in the royalblue module. (**G**) Trajectory of the MEs in the royalblue module between Ctrl-APOE4 and αSyn-APOE4 mice. (**H**) GO term enrichment of the blue module using 4107 module genes. (**I**) Network plot of the top 10 hub genes in the blue module. (**J**) Trajectory of the MEs in the blue module between Ctrl-APOE4 and αSyn-APOE4 mice. Student's *t* tests were used. $^{**}P < 0.01$.

that *APOE4* may alter the risk of DLB and PDD through a direct effect on Lewy body pathology. A pure synucleinopathy animal model without the presence of amyloid offers an opportunity to study direct effects of APOE4 on α-synuclein pathology. The dosage of *SNCA* has been known to be responsible for α-synuclein pathology in humans and mouse models (*22*, *23*). We thus overexpressed human α-synuclein with viral delivery in humanized mouse models for each *APOE* allele (*APOE2*, *APOE3*, and *APOE4*). In these synucleinopathy mouse models, we observed not only more severe α-synuclein pathology and neurodegeneration but also behavioral deficits in the presence of *APOE4*. In support of the validity of the findings from animal models, the burden of both p-S129 and conformationally changed (immunoreactive for 5G4 antibody) α-synuclein as measured with digital microscopy and image analysis was greater in patients with LBD with minimal Alzheimer type pathology (Thal amyloid phase ≤ 1 and Braak neurofibrillary tangle stage ≤ III) if they carried an *APOE4* allele. Together, our results support a direct effect of *APOE4* on α-synuclein pathology and related toxicity, in addition to indirect effects of *APOE4*-associated Alzheimer pathology on α-synuclein pathology.

APOE is primarily expressed by astrocytes in the brain, and it delivers cholesterol and other lipids to neurons through APOE receptors, including the low-density lipoprotein receptor (LDLR) and low-density lipoprotein receptor–related protein 1 (LRP1) (*14*). The three human APOE isoforms (APOE2, APOE3, and APOE4) differ from one another only at residues 112 and 158 (*15*); however, these single–amino acid polymorphisms substantially alter the structure and function of APOE, modulating its binding properties to both lipids and its receptors. It is worth noting that α-synuclein is also a lipid-binding protein, and it has an apolipoprotein-like lipid-binding domain within its N terminus (*45*), a domain in which most of the coding region mutations that give rise to LBD are located (*46*).

There are various hypotheses on physiological functions of α-synuclein, one of which is to bind to plasma membranes through its lipid-binding domain to maintain a synaptic vesicle reserve pool within presynaptic terminals, which promotes synaptic vesicle docking, release, and recycling (*18*). There is also evidence to suggest a direct role of α-synuclein in brain lipid metabolism given that it is found in lipoprotein particles in cerebrospinal fluid (*47*, *48*).

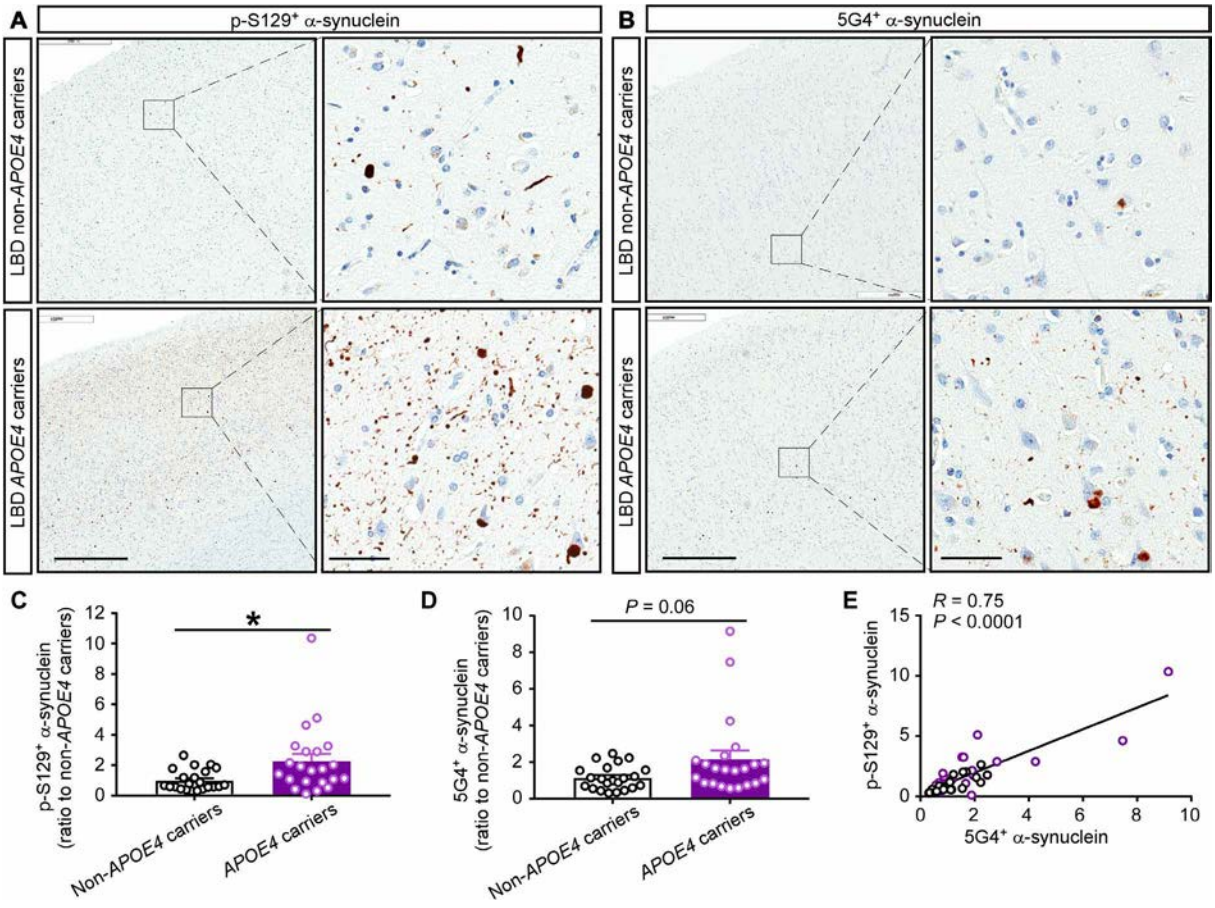

Fig. 7. Increased α-synuclein pathology in the human postmortem brains of *APOE4* carriers with LBD and minimal AD type pathology. Human postmortem brain sections from LBD cases were prepared as described in Materials and Methods. The p-S129 phosphorylated α-synuclein and conformationally changed pathogenic α-synuclein were determined by immunohistochemical staining with pSyn#63 and 5G4 antibodies, respectively. Representative images are shown for the deposition of p-S129–positive (**A**) and 5G4-positive (**B**) pathogenic α-synuclein in the superior temporal cortex of *APOE4* carriers and noncarriers. Scale bars, 600 μm (left) and 50 μm (right) in both (A) and (B). The immunoreactivities of p-S129 staining (**C**) and 5G4 staining (**D**) were evaluated and quantified by Aperio ImageScope ($n = 22$ cases per group). Data represent means ± SEM relative to non-*APOE4* carriers. Mann-Whitney *U* tests were used. *$P < 0.05$. (**E**) The correlation between p-S129 and 5G4 immunoreactivities in all the cases was determined by Spearman correlation tests. The black and purple circles represent non-*APOE4* carriers and *APOE4* carriers, respectively.

In our αSyn-APOE4 models, we observed abnormal behaviors affecting memory and motor functions, as well as evidence of synaptic loss and gliosis. Dysregulation of synapse-related pathways may indicate that physiological functions of α-synuclein are more likely to be disrupted by the presence of APOE4. Alternatively, increased α-synuclein pathology might be independent or synergistic with APOE4-related neurotoxicity. Molecular profiling of these models revealed that lipid metabolic pathways were impaired in αSyn-APOE4 mice. Because both α-synuclein and APOE4 can bind to lipids, it is possible that APOE4 might compete with α-synuclein for membrane lipid binding and thus negatively affect synaptic function and lipid metabolism. As such, alterations in membrane and lipoprotein homeostasis associated with APOE4 might contribute to neurotoxicity of α-synuclein in LBD. It is worth noting that APOE4 is associated with impairments in both peripheral (*49*) and central (*50*) lipid metabolism and that α-synuclein is one of the few proteins associated with neurodegeneration that is also present in peripheral nervous system (*51*). Future studies should be directed to addressing how genotype-specific effects of *APOE* affect lipid homeostasis in LBD.

There is also evidence supporting a direct physical interaction between α-synuclein and APOE (*52*–*54*), although more investigation is needed to address APOE isoform–specific effects and their relevance in human disease. It is generally agreed that intracellular aggregation of α-synuclein plays a crucial role in the pathogenesis of LBD; however, a rapidly growing body of evidence suggests that small amounts of α-synuclein are released from neurons by unconventional exocytosis and that this extracellular α-synuclein pool may contribute to the pathogenesis of LBD, especially because it relates to spreading or intercellular propagation of α-synuclein (*55*). Because APOE is a naturally secreted protein that is readily detected in the extracellular fluids at relatively high concentrations (*56*, *57*), it is possible that APOE interacts with extracellular α-synuclein, modulating its release, uptake, and clearance. Because *APOE4* is a genetic risk factor for PDD, but not necessarily PD, it is tempting to speculate that effects of APOE4 manifest more in neocortex where AD and LBD pathologies are found, whereas it has minimal impact on subcortical or brainstem structures where Lewy pathology is predominant in PD. As such, APOE4 might modify spread of extracellular α-synuclein to cortical regions. The exact mechanisms by which APOE isoforms

differentially regulate α-synuclein metabolism, aggregation, and toxicity under normal and pathological conditions remain to be determined.

We found three genes affected by α-synuclein pathology in all αSyn-APOE mice, including *Ak7*, *Spata18*, *and Grp*. *Ak7* encodes a member of the adenylate kinase family. Adenylate kinase and downstream adenosine monophosphate (AMP) signaling act as an integrated metabolic monitoring system that reads cellular energy states to tune and report signals to metabolic sensors (*58*). A recent study demonstrated that a mutation in *AK7* is associated with hydrocephalus and a primary ciliary dyskinesia phenotype in chronic obstructive pulmonary disease (*59*); however, the exact biological function of Ak7 in the brain remains unclear. *Spata18* is a p53-inducible gene that encodes mitochondria-eating protein (Mieap) in the mitochondrial matrix (*60*). Mieap is a key regulator of mitochondrial quality that mediates repair or degradation of unhealthy mitochondria in response to mitochondrial damage (*60*–*62*). In response to stress, Mieap is induced and translocates to the mitochondrial matrix in a reactive oxygen species–dependent manner (*61*), allowing lysosomal enzymes to move into the matrix and to degrade oxidatively damaged mitochondrial proteins. Gastrin-releasing peptide (GRP), encoded by *Grp* gene, is a mammalian neuropeptide that binds to the GRP receptor. Alterations in GRP or GRP receptor expression or function have been reported in neurodegenerative disorders (*63*). The mechanisms of how these three genes and related pathways are linked to α-synuclein expression are yet to be defined.

In addition to amyloid pathology in AD and α-synuclein pathology in LBD, APOE4 has also been shown to affect other proteinopathies in neurodegenerative diseases. APOE4 has been shown to exacerbate neurodegeneration and neuroinflammation in a tau transgenic mouse model (*64*). *APOE4* has been associated with increased TDP-43 pathology independent of Aβ in AD (*65*, *66*). Most recently, APOE4 has been associated with lower age of onset of frontotemporal degenerations and tauopathies independent of Aβ (*67*). This growing evidence highlights the damaging effects of APOE4 in chronic neurodegenerative conditions, especially those linked to dementia.

Our study has several limitations. Although we demonstrate the effect of APOE4 on exacerbating α-synuclein pathology in a model system and identified several potential pathways by transcriptomic profiling, the exact molecular mechanism driving the APOE4-specific effects is not clear. Next, although α-synuclein pathology and neurodegeneration were observed using this AAV-mediated *SNCA* overexpression mouse model, our model does not recapitulate all features of the human disease and pathology. For instance, CA2/3 is usually cited as the predominant site of hippocampal Lewy pathology, whereas CA1 is less affected in human LBD brains (*68*, *69*). However, in our mouse model, the α-synuclein pathology was mainly found in the CA1 subregion of the hippocampus. In addition, the cognitive and psychiatric changes in LBD are linked in a variety of ways to alterations in multiple neurotransmitter systems including dopaminergic, serotonergic, noradrenergic, and cholinergic systems (*70*–*72*). However, it is unclear which deficits of neurotransmitter systems occur in our models and how APOE affects these pathways. Last, although beyond the scope of this current study, the interactive contribution of amyloid or tau pathologies to the impact of APOE4 on pathologic α-synuclein formation is not addressed in our study and needs further investigation.

In summary, our study supports a pathogenic role of APOE4 in promoting α-synuclein pathology independent of amyloid pathology both in mouse models and in LBD. These findings provide insights into the role of APOE4 in α-synuclein metabolism and aggregation in LBD that may guide future clinical trial designs and early prevention strategies for LBD.

MATERIALS AND METHODS

Study design

This study aimed to investigate how APOE isoforms differentially modulate synucleinopathy using AAV-based α-synuclein mouse model and human pathological analysis. To accomplish this, we expressed human wild-type α-synuclein protein in human APOE-TR mouse by using AAV–α-synuclein injection (αSyn) into both cerebral ventricles of APOE-TR pups on postnatal day 0, with the AAV expressing GFP as a Ctrl. The mice were selected randomly for AAV-αSyn or AAV-GFP injection. The effects of APOE isoforms on synuclein pathology, behavior, neuronal and synaptic integrity, gliosis, as well as transcriptomic signatures were assessed at 9 months of age. Transcriptomic profiling was performed to address potential underlying pathways. To address human relevance, we analyzed α-synuclein pathology in LBD with respect to *APOE4* genotype. Mice with different *APOE* genotypes and AAV injection protocols were selected on the basis of available experimental tools and techniques used previously by our investigative team. Twelve to 21 mice per genotype per group were injected with AAV vectors and were used for behavioral tests and immunostaining. Six mice per genotype were randomly selected for biochemical analysis. Sample sizes were adequately powered to observe the effects on the basis of past experience (*26*, *73*–*76*) and preliminary studies. Human subjects were chosen at random, matching for age and sex as closely as possible. The behavioral tests were conducted blinded to genotype and AAV transgene expression by experienced technicians. Immunohistochemistry, digital microscopy, and image analysis were performed blinded to genotype and AAV transgene expression. All the data collection and the quantification were performed by investigators unaware of sample identities until unblinding for final interpretation of statistical results.

Animals

APOE-TR mice in which murine *ApoE* gene locus is replaced with human *APOE* ε2/ε2, *APOE* ε3/ε3, or *APOE* ε4/ε4 gene were obtained from Taconic Laboratories, Rensselaer, NY (APOE2, model #1547; APOE3, model #1548; APOE4, model #1549). All mice were on C57BL/6 background. Animals were housed under controlled temperature and lighting conditions and were given free access to food and water. All animal procedures were approved by the Mayo Clinic Institutional Animal Care and Use Committee and were in accordance with the National Institutes of Health *Guide for the Care and Use of Laboratory Animals*.

Intracerebroventricular viral injections in animals

Human α-synuclein or GFP expression plasmids in AAV2/1 vectors (abbreviated as AAV-αSyn and AAV-GFP, respectively) were prepared as previously reported (*27*). Briefly, AAV serotype 2/1 vectors expressing full-length human wild-type α-synuclein or GFP under the control of the cytomegalovirus enhancer/chicken β-actin promoter were generated by plasmid triple transfection with helper plasmids in human embryonic kidney (HEK) 293T cells. Forty-eight hours later, cells were harvested and lysed in the presence of 0.5% sodium deoxycholate and benzonase (50 U/ml; Sigma-Aldrich) by freeze thawing, and the viruses were isolated using a discontinuous iodixanol gradient. The constructs were sequence-verified using ABI3730 with

BigDye chemistry following the manufacturer's protocols (Applied Biosystems, Foster City). The genomic titer of each virus was determined by qPCR. APOE2-TR, APOE3-TR, and APOE4-TR pups at postnatal day 0 underwent intracerebroventricular injection with 2 μl of AAV-GFP or AAV-αSyn into both hemispheres as aforementioned (*26*). Newborn pups were cryoanesthetized and subsequently placed on a cold metal plate. A 30-gauge needle was used to pierce the skull just posterior to bregma and 2 mm lateral to the midline, and AAV vector sample was injected into the lateral ventricles. The pups in each breeder were randomly selected to receive either AAV-GFP or AAV-αSyn injections.

Behavioral tests

A behavioral battery consisting of OFA, EPM, contextual and cued fear conditioning (CFC) tests, hindlimb clasping tests, hangwire tests, and the rotarod tests were performed in 9-month-old Ctrl-APOE and αSyn-APOE mice as described (*26*, *77*–*80*). In OFA tests, mice were placed in the center of an open-field arena (40 cm × 40 cm × 30 cm, $W \times L \times H$). The total distance traveled, average speed, time mobile, and distance traveled in an imaginary "center" zone (20 cm × 20 cm) were measured. In the EPM tests, the entire maze was elevated 50 cm from the floor. Mice were tested by being placed in the center of the maze, facing an open arm, and their behavior was tracked for 5 min. The CFC tests were conducted in a sound-attenuating chamber with a grid floor capable of delivering an electric shock. Mice were initially placed into the chamber undisturbed for 2 min, during which the baseline freezing behavior was recorded. An 80-dB white noise served as the conditioned stimulus (CS) and was presented for 30 s. During the final 2 s of this noise, mice received a mild foot shock (0.5 mA), which served as the unconditioned stimulus (US). After 1 min, another CS-US pair was presented. The mouse was removed 30 s after the second CS-US pair before being returned to their home cages. Twenty-four hours later, each mouse was returned to the test chamber and freezing behavior was recorded for 5 min (context test). For the auditory CS test, environmental and contextual cues were changed as described (*26*). The animals were placed in the apparatus for 3 min and then the auditory CS was presented, and freezing was recorded for another 3 min (cued test). Baseline freezing behavior obtained during training was subtracted from the context or cued tests to serve as a control for animal variability. For hindlimb clasping test, the mice were suspended by their tail and the extent of hindlimb clasping was observed for 30 s. If both hindlimbs were splayed outward away from the abdomen with splayed toes, a score of 0 was given. If one hindlimb was retracted or both hindlimbs were partially retracted toward the abdomen without touching it and the toes were splayed, a score of 1 was assigned. If both hindlimbs were partially retracted toward the abdomen and were touching the abdomen without touching each other, a score of 2 was given. If both hindlimbs were fully clasped and touching the abdomen, a score of 3 was assigned (*79*, *80*). The balance and grip strength were evaluated with hangwire tests. Briefly, mice were hung upside down on a wire 50 cm above a mouse cage (*78*, *80*). The time until the mouse fell off the wire and into the cage was recorded as latency to fall off. The mice were then put back on the wire, and the total numbers of fall off were recorded within 2 min of trial period. Mice that did not fall off within 2 min were removed and assigned a maximal time of 2 min (*80*). The rotarod tests were performed as previously reported (*77*), with mice given four trials per day for four consecutive days. Latency to fall off from the rotarod was averaged for each trial per day.

Tissue preparation

Mice were deeply anesthetized with isoflurane before transcardial perfusion with saline. The brain was removed and bisected along the midline. One half was drop-fixed in 10% neutral buffered formalin (Fisher Scientific) overnight at 4°C for histology, and the other half was snap-frozen in liquid nitrogen and stored at −80°C. For biochemical analysis, the brain tissues were homogenized and lysed in RAB (100 mM MES, 1 mM EDTA, 0.5 mM $MgSO_4$, 750 mM NaCl, 20 mM NaF, and 1 mM Na_3VO_4) (G-Biosciences), supplemented with protease inhibitor (cOmplete) and phosphatase inhibitor (PhosSTOP) (Roche). The samples were ultracentrifuged at 50,000*g* for 20 min at 4°C. The supernatants were collected as RAB-soluble fractions. The pellets were resuspended in RIPA (Fisher Scientific), supplemented with protease inhibitor (cOmplete) and phosphatase inhibitor (PhosSTOP), and ultracentrifuged at 50,000*g* for 20 min at 4°C. The supernatants were collected as RIPA-soluble fractions. The pellets were resuspended and sonicated in 2% SDS buffer (Sigma-Aldrich) and then centrifuged at 50,000*g* for 20 min at 4°C. The supernatants were collected as SDS fractions. All fractions were stored at −80°C until they were used for Western blot and ELISA analysis.

Western blotting

Equal amounts of protein from the RAB, RIPA, and SDS fractions of homogenized tissue lysates were resolved by SDS–polyacrylamide gel electrophoresis and transferred to polyvinylidene difluoride membranes. After the membranes were blocked, proteins of interest were detected with a primary antibody. The membrane was then probed with a horseradish peroxidase–conjugated secondary antibody and visualized using the Odyssey Infrared Imaging System (LI-COR). The following primary antibodies were used: anti-GluR2 (catalog no. MAB397, Millipore, 1:1000), anti-PSD95 (catalog no. 3450s, Cell Signaling Technology, 1:1000), anti-NR2A (catalog no. 05-901R, Millipore, 1:1000), anti–α-synuclein (catalog no. 807801, BioLegend, 1:1000), anti-APOE (catalog no. K74180B, Meridian Life Science, 1:1000), anti-GFAP (catalog no. MAB360, Millipore, 1:1000), anti–β-tubulin (catalog no. T8328, Sigma-Aldrich, 1:5000), and anti–β-actin (catalog no. A2228, Sigma-Aldrich, 1:2000) antibodies.

α-Synuclein ELISA

The α-synuclein ELISA was carried out using a commercial ELISA kit (catalog no. AS-55550-H, AnaSpec) according to the manufacturer's instructions. Briefly, 100 μl of samples and 50 μl of detection antibodies were added into the antibody-coated plate and incubated for 4 hours at room temperature. After washing, the plate was incubated with 100 μl of 3,3′,5,5′-tetramethylbenzidine (TMB) for 10 min and 50 μl of the Stop Solution before colorimetric absorbance measurements were taken at 450 nm using a Synergy HT plate reader (BioTek).

RNA sequencing

Quality control and normalization

Total RNA was isolated using TRIzol reagent (Qiagen) and RNeasy Mini Kit (Qiagen) and was subjected to deoxyribonuclease I digestion to remove contaminating genomic DNA. The mRNA samples were sequenced at Mayo Clinic using Illumina HiSeq 4000. Reads were mapped to the mouse genome mm10. The raw gene read counts, along with sequencing quality control, were generated using the Mayo Clinic RNA sequencing (RNA-seq) analytic pipeline: MAP-RSeq version 3.0.1 (*81*). Conditional quantile normalization (CQN) was performed on raw gene counts to remove biases created by GC content

and technical variation, to adjust for gene length and library size differences, and to obtain similar quantile-by-quantile distributions of gene expression across samples (*82*). On the basis of the bimodal distribution of the CQN-normalized and $\log_2$-transformed reads per kilobase per million (RPKM) gene expression values, genes with average $\log_2$ RPKM ≥ 2 in at least one group was considered to have expression above the detection threshold. Using this selection threshold, 19,005 genes were included in downstream analyses.

Differential gene expression and pathway analysis

Differential gene expression analysis was performed using Partek Genomics Suite (Partek Inc.). On the basis of the source of variation analysis, sequence coverage, flowcell, and sex were main contributors to the variation of gene expression and thus were included as factors in the analysis of variance (ANOVA) model. The Benjamini-Hochberg procedure (Benjamini-Hochberg step-up procedure) was used to adjust for multiple testing. Pathway enrichment analyses were performed using MetaCore (Thomson Reuters) (version 6.25) and Ingenuity Pathway Analysis (Qiagen Inc.; www.qiagenbioinformatics.com/products/ingenuitypathway-analysis).

Weighted gene coexpression network analysis

To identify groups of genes that are correlated with α-synuclein overexpression, we performed WGCNA (*83*) using residual expression values calculated by adjusting for sequence coverage, flowcell, and sex, all of which contributed substantially to the variation of gene expression. WGCNA was performed for APOE4 datasets. Signed hybrid coexpression networks were built for all WGCNAs. On the basis of the relationships between power and scale independence, the power of 10 was chosen for building scale-free topology for all three datasets. We used hybrid dynamic tree cutting, a minimum module size of 60 genes, and a minimum height for merging modules at 0.4. To assess the correlation of modules with treatment, we defined Ctrl-APOE4 as 0 and αSyn-APOE4 as 1. Modules significantly correlated with the treatment were annotated using R package anRichment (https://horvath.genetics.ucla.edu/html/CoexpressionNetwork/GeneAnnotation/index.html). Selected networks were visualized using VisANT (*84*).

qPCR analysis

Reverse transcription of RNA was performed using iScript Reverse Transcription Supermix (Bio-Rad). Complementary DNA was added to a reaction mix (20-μl final volume) containing gene-specific primers and SYBR Green Supermix (Bio-Rad). All samples were run in duplicate and were analyzed with CFX96 Real-Time PCR Detection System (Bio-Rad). The relative gene expression was normalized to *Gapdh* expression and assessed using the $2^{-\Delta\Delta CT}$ method. Primer sequences and information are as follows: *Gapdh*, 5′-AGGTCGGTGTGAACGGATTTG-3′ (forward) and 5′-TGTAGACCATGTAGTTGAGGTCA-3′ (reverse); *Gfap*, 5′-GCACTCAATACGAGGCAGTG-3′ (forward) and 5′-GGCGATAGTCGTTAGCTTCG-3′ (reverse); *Igf2*, 5′-GTCGATGTTGGTGCTTCTCATC-3′ (forward) and 5′-GGGTATCTGGGGAAGTCGT-3′ (reverse); *Ppp1r3g*, 5′-CTTTCACGGAGTGGCGTACCTT-3′ (forward) and 5′-AGGCACAGCGAGAAGTGGAAAC-3′ (reverse); human *APOE*, 5′-TGTCTGAGCAGGTGCAGGAG-3′ (forward) and 5′-TCCAGTTCCGATTTGTAGG-3′ (reverse); *Prkcd*, 5′-GGAGCAAACCAGGGCAGACGGGCCTACTCT-3′ (forward) and 5′-GGGGTCCTCCTGTACGAAATGCTCATCGGC-5′ (reverse); *Cyr61*, 5′-CAGCTCACTGAAGAGGCTTC-3′ (forward) and 5′-GCGTGCAGAGGGTTGAAAAG-3′ (reverse); *Spata18*, Mm.PT.58.7498900 [Integrated Device Technology (IDT), CA]; *Ak7*, Mm.PT.58.33384033 (IDT); *Grp*, Mm.PT.58.41177438 (IDT); *Snca*, Mm.PT.58.8495900 (IDT); *Human SNCA*, Hs.PT.58.912923 (IDT); *Apoc1*, Mm.PT.58.10342960 (IDT).

Human LBD postmortem brain α-synuclein pathology analysis

The LBD brains were obtained from the Mayo Clinic Brain Bank for Neurodegenerative Disorders, which operates under procedures approved by the Mayo Clinic Institutional Review Board. The LBD brains were evaluated with standardized histopathological methods as described (*39*). In this study, only LBD cases with minimal Alzheimer type pathology (Braak stages 0 to III and Thal phases 0 to 1) and known *APOE* genotype were included. Image analysis of p-S129 and conformationally changed α-synuclein (5G4) immunostained sections included 22 cases of *APOE4* carriers and 22 cases of age- and sex-matched *APOE4* noncarriers. Characteristics of the LBD cases are shown in table S1.

Histology and immunohistochemistry

The brain sample was fixed in 10% formalin and embedded in paraffin wax, sectioned in a coronal plane at 5-μm thickness, and mounted on glass slides. Sections were collected from the same brain region for all the animals, and brain regions were confirmed under the microscope by comparing sections to images on the Allen Mouse Brain Atlas site (Allen Institute for Brain Science, 2004). The tissue sections were deparaffinized in xylene and rehydrated in a graded series of alcohols. Antigen retrieval was performed by steaming in distilled water for 30 min, and endogenous peroxidase activity was blocked by incubation in 0.03% hydrogen peroxide. Sections were then immunostained using the Dako Autostainer and the Dako EnVision+ System, HRP. The stained slides were dehydrated, coverslipped, and scanned with the Aperio Slide Scanner (Aperio). The following primary antibodies were used: anti-GFAP (catalog no. Pu020-UP, BioGenex, 1:2500), anti-IBA1 (catalog no. 019-19741, Wako, 1:2500), anti-CD68 (catalog no. ab125212, Abcam, 1:2500), anti-NeuN (catalog no. MAB377, clone A60, Millipore, 1:5000), anti–conformationally changed α-synuclein (catalog no. MABN389, clone 5G4, Millipore, 1:10,000), anti–phosphorylated α-synuclein (catalog no. 015-25191, #pSyn64, Wako, 1:10,000), and anti–total α-synuclein (catalog no. 807801, BioLegend, 1:10,000). A technician blinded to genotype and AAV status performed immunohistochemical staining. Data collection and quantification of immunoreactivity were performed by another technician blindly.

Statistical analyses

All data were reported as means ± SEM (unless elsewise indicated). To ensure that results were valid in the presence of non-normal distributions or differing variances between groups, nonparametric Mann-Whitney *U* tests were used to compare outcomes between Ctrl and αSyn mice separately for APOE2, APOE3, and APOE4 groups, and Kruskal-Wallis tests with Dunn's multiple comparison tests were used to compare outcomes among αSyn-APOE2, αSyn-APOE3, and αSyn-APOE4 groups. With the sample size $n = 6$, Student's *t* tests were used to compare outcomes between Ctrl and αSyn mice. All statistical tests were two-sided. In the captions of the figures, we reported the used statistical tests for each analysis, the numerosity of the experiments, and the significance levels. In the Supplementary Materials, the raw data with less than 20 samples are reported.

SUPPLEMENTARY MATERIALS

stm.sciencemag.org/cgi/content/full/12/529/eaay1809/DC1

Fig. S1. Widespread expression of human α-synuclein protein in the brain of αSyn-APOE mice.
Fig. S2. Widespread expression of GFP in the brain of Ctrl-APOE mice.
Fig. S3. Expression of human and mouse α-synuclein in the brain of Ctrl-APOE and αSyn-APOE mice.
Fig. S4. α-Synuclein pathology in the substantia nigra region of αSyn-APOE4 mice.
Fig. S5. Increased phosphorylated α-synuclein in αSyn-APOE4 mice.
Fig. S6. Solubility of human α-synuclein in the brain of Ctrl-APOE and αSyn-APOE mice.
Fig. S7. Solubility of total α-synuclein in the brain of Ctrl-APOE and αSyn-APOE mice.
Fig. S8. Behavioral abnormalities in αSyn-APOE mice.
Fig. S9. Correlation of behavioral performances and α-synuclein pathologies in αSyn-APOE mice.
Fig. S10. Correlation of neurodegeneration and astrogliosis with α-synuclein pathologies in αSyn-APOE mice.
Fig. S11. Microglial marker expression in αSyn-APOE mice.
Fig. S12. DEGs and related pathways between Ctrl-APOE and αSyn-APOE mice in different *APOE* genetic backgrounds identified by transcriptomic profiling.
Fig. S13. Pathways specifically affected in APOE4-TR mice upon human α-synuclein expression.
Fig. S14. Glia marker expression in human LBD brain.
Table S1. Patient characteristics for LBD cohort.
Data file S1. Raw data for all the figures where $n < 20$.

View/request a protocol for this paper from *Bio-protocol*.

REFERENCES AND NOTES

1. T. Rahkonen, U. Eloniemi-Sulkava, S. Rissanen, A. Vatanen, P. Viramo, R. Sulkava, Dementia with Lewy bodies according to the consensus criteria in a general population aged 75 years or older. *J. Neurol. Neurosurg. Psychiatry* **74**, 720–724 (2003).
2. M. Emre, Dementia associated with Parkinson's disease. *Lancet Neurol.* **2**, 229–237 (2003).
3. C. F. Lippa, J. E. Duda, M. Grossman, H. I. Hurtig, D. Aarsland, B. F. Boeve, D. J. Brooks, D. W. Dickson, B. Dubois, M. Emre, S. Fahn, J. M. Farmer, D. Galasko, J. E. Galvin, C. G. Goetz, J. H. Growdon, K. A. Gwinn-Hardy, J. Hardy, P. Heutink, T. Iwatsubo, K. Kosaka, V. M.-Y. Lee, J. B. Leverenz, E. Masliah, I. G. McKeith, R. L. Nussbaum, C. W. Olanow, B. M. Ravina, A. B. Singleton, C. M. Tanner, J. Q. Trojanowski, Z. K. Wszolek; DLB/PDD Working Group, DLB and PDD boundary issues: Diagnosis, treatment, molecular pathology, and biomarkers. *Neurology* **68**, 812–819 (2007).
4. I. G. McKeith, B. F. Boeve, D. W. Dickson, G. Halliday, J.-P. Taylor, D. Weintraub, D. Aarsland, J. Galvin, J. Attems, C. G. Ballard, A. Bayston, T. G. Beach, F. Blanc, N. Bohnen, L. Bonanni, J. Bras, P. Brundin, D. Burn, A. Chen-Plotkin, J. E. Duda, O. El-Agnaf, H. Feldman, T. J. Ferman, D. Ffytche, H. Fujishiro, D. Galasko, J. G. Goldman, S. N. Gomperts, N. R. Graff-Radford, L. S. Honig, A. Iranzo, K. Kantarci, D. Kaufer, W. Kukull, V. M. Y. Lee, J. B. Leverenz, S. Lewis, C. Lippa, A. Lunde, M. Masellis, E. Masliah, P. McLean, B. Mollenhauer, T. J. Montine, E. Moreno, E. Mori, M. Murray, J. T. O'Brien, S. Orimo, R. B. Postuma, S. Ramaswamy, O. A. Ross, D. P. Salmon, A. Singleton, A. Taylor, A. Thomas, P. Tiraboschi, J. B. Toledo, J. Q. Trojanowski, D. Tsuang, Z. Walker, M. Yamada, K. Kosaka, Diagnosis and management of dementia with Lewy bodies: Fourth consensus report of the DLB Consortium. *Neurology* **89**, 88–100 (2017).
5. I. J. Siddiqui, N. Pervaiz, A. A. Abbasi, The Parkinson disease gene SNCA: Evolutionary and structural insights with pathological implication. *Sci. Rep.* **6**, 24475 (2016).
6. E. Sidransky, M. A. Nalls, J. O. Aasly, J. Aharon-Peretz, G. Annesi, E. R. Barbosa, A. Bar-Shira, D. Berg, J. Bras, A. Brice, C. M. Chen, L. N. Clark, C. Condroyer, E. V. de Marco, A. Dürr, M. J. Eblan, S. Fahn, M. J. Farrer, H.-C. Fung, Z. Gan-Or, T. Gasser, R. Gershoni-Baruch, N. Giladi, A. Griffith, T. Gurevich, C. Januario, P. Kropp, A. E. Lang, G.-J. Lee-Chen, S. Lesage, K. Marder, I. F. Mata, A. Mirelman, J. Mitsui, I. Mizuta, G. Nicoletti, C. Oliveira, R. Ottman, A. Orr-Urtreger, L. V. Pereira, A. Quattrone, E. Rogaeva, A. Rolfs, H. Rosenbaum, R. Rozenberg, A. Samii, T. Samaddar, C. Schulte, M. Sharma, A. Singleton, M. Spitz, E.-K. Tan, N. Tayebi, T. Toda, A. R. Troiano, S. Tsuji, M. Wittstock, T. G. Wolfsberg, Y.-R. Wu, C. P. Zabetian, Y. Zhao, S. G. Ziegler, Multicenter analysis of glucocerebrosidase mutations in Parkinson's disease. *N. Engl. J. Med.* **361**, 1651–1661 (2009).
7. G. Berge, S. B. Sando, A. Rongve, D. Aarsland, L. R. White, Apolipoprotein E ε2 genotype delays onset of dementia with Lewy bodies in a Norwegian cohort. *J. Neurol. Neurosurg. Psychiatry* **85**, 1227–1231 (2014).
8. J. Bras, R. Guerreiro, L. Darwent, L. Parkkinen, O. Ansorge, V. Escott-Price, D. G. Hernandez, M. A. Nalls, L. N. Clark, L. S. Honig, K. Marder, W. M. van der Flier, A. Lemstra, P. Scheltens, E. Rogaeva, P. St George-Hyslop, E. Londos, H. Zetterberg, S. Ortega-Cubero, P. Pastor, T. J. Ferman, N. R. Graff-Radford, O. A. Ross, I. Barber, A. Braae, K. Brown, K. Morgan, W. Maetzler, D. Berg, C. Troakes, S. Al-Sarraj, T. Lashley, Y. Compta, T. Revesz, A. Lees, N. Cairns, G. M. Halliday, D. Mann, S. Pickering-Brown, D. W. Dickson, A. Singleton, J. Hardy, Genetic analysis implicates APOE, SNCA and suggests lysosomal dysfunction in the etiology of dementia with Lewy bodies. *Hum. Mol. Genet.* **23**, 6139–6146 (2014).
9. R. Guerreiro, O. A. Ross, C. Kun-Rodrigues, D. G. Hernandez, T. Orme, J. D. Eicher, C. E. Shepherd, L. Parkkinen, L. Darwent, M. G. Heckman, S. W. Scholz, J. C. Troncoso, O. Pletnikova, O. Ansorge, J. Clarimon, A. Lleo, E. Morenas-Rodriguez, L. Clark, L. S. Honig, K. Marder, A. Lemstra, E. Rogaeva, P. St George-Hyslop, E. Londos, H. Zetterberg, I. Barber, A. Braae, K. Brown, K. Morgan, C. Troakes, S. Al-Sarraj, T. Lashley, J. Holton, Y. Compta, V. van Deerlin, G. E. Serrano, T. G. Beach, S. Lesage, D. Galasko, E. Masliah, I. Santana, P. Pastor, M. Diez-Fairen, M. Aguilar, P. J. Tienari, L. Myllykangas, M. Oinas, T. Revesz, A. Lees, B. F. Boeve, R. C. Petersen, T. J. Ferman, V. Escott-Price, N. Graff-Radford, N. J. Cairns, J. C. Morris, S. Pickering-Brown, D. Mann, G. M. Halliday, J. Hardy, J. Q. Trojanowski, D. W. Dickson, A. Singleton, D. J. Stone, J. Bras, Investigating the genetic architecture of dementia with Lewy bodies: A two-stage genome-wide association study. *Lancet Neurol.* **17**, 64–74 (2018).
10. D. Tsuang, J. B. Leverenz, O. L. Lopez, R. L. Hamilton, D. A. Bennett, J. A. Schneider, A. S. Buchman, E. B. Larson, P. K. Crane, J. A. Kaye, P. Kramer, R. Woltjer, J. Q. Trojanowski, D. Weintraub, A. S. Chen-Plotkin, D. J. Irwin, J. Rick, G. D. Schellenberg, G. S. Watson, W. Kukull, P. T. Nelson, G. A. Jicha, J. H. Neltner, D. Galasko, E. Masliah, J. F. Quinn, K. A. Chung, D. Yearout, I. F. Mata, J. Y. Wan, K. L. Edwards, T. J. Montine, C. P. Zabetian, APOE ε4 increases risk for dementia in pure synucleinopathies. *JAMA Neurol.* **70**, 223–228 (2013).
11. X. Huang, P. Chen, D. I. Kaufer, A. I. Tröster, C. Poole, Apolipoprotein E and dementia in Parkinson disease: A meta-analysis. *Arch. Neurol.* **63**, 189–193 (2006).
12. D. J. Irwin, M. T. White, J. B. Toledo, S. X. Xie, J. L. Robinson, V. van Deerlin, V. M.-Y. Lee, J. B. Leverenz, T. J. Montine, J. E. Duda, H. I. Hurtig, J. Q. Trojanowski, Neuropathologic substrates of Parkinson disease dementia. *Ann. Neurol.* **72**, 587–598 (2012).
13. C.-C. Liu, T. Kanekiyo, H. Xu, G. Bu, Apolipoprotein E and Alzheimer disease: Risk, mechanisms and therapy. *Nat. Rev. Neurol.* **9**, 106–118 (2013).
14. G. Bu, Apolipoprotein E and its receptors in Alzheimer's disease: Pathways, pathogenesis and therapy. *Nat. Rev. Neurosci.* **10**, 333–344 (2009).
15. N. Zhao, C.-C. Liu, W. Qiao, G. Bu, Apolipoprotein E, receptors, and modulation of Alzheimer's disease. *Biol. Psychiatry* **83**, 347–357 (2018).
16. M. G. Spillantini, M. L. Schmidt, V. M.-Y. Lee, J. Q. Trojanowski, R. Jakes, M. Goedert, α-Synuclein in Lewy bodies. *Nature* **388**, 839–840 (1997).
17. K. Vekrellis, M. Xilouri, E. Emmanouilidou, H. J. Rideout, L. Stefanis, Pathological roles of α-synuclein in neurological disorders. *Lancet Neurol.* **10**, 1015–1025 (2011).
18. H. A. Lashuel, C. R. Overk, A. Oueslati, E. Masliah, The many faces of α-synuclein: From structure and toxicity to therapeutic target. *Nat. Rev. Neurosci.* **14**, 38–48 (2013).
19. M. Farrer, F. Wavrant-De Vrieze, R. Crook, L. Boles, J. Perez-Tur, J. Hardy, W. G. Johnson, J. Steele, D. Maraganore, K. Gwinn, T. Lynch, Low frequency of α-synuclein mutations in familial Parkinson's disease. *Ann. Neurol.* **43**, 394–397 (1998).
20. R. Krüger, W. Kuhn, T. Müller, D. Woitalla, M. Graeber, S. Kösel, H. Przuntek, J. T. Epplen, L. Schols, O. Riess, AlaSOPro mutation in the gene encoding α-synuclein in Parkinson's disease. *Nat. Genet.* **18**, 106–108 (1998).
21. R. A. Fredenburg, C. Rospigliosi, R. K. Meray, J. C. Kessler, H. A. Lashuel, D. Eliezer, P. T. Lansbury, The impact of the E46K mutation on the properties of α-synuclein in its monomeric and oligomeric States. *Biochemistry* **46**, 7107–7118 (2007).
22. M. C. Chartier-Harlin, J. Kachergus, C. Roumier, V. Mouroux, X. Douay, S. Lincoln, C. Levecque, L. Larvor, J. Andrieux, M. Hulihan, N. Waucquier, L. Defebvre, P. Amouyel, M. Farrer, A. Destée, α-Synuclein locus duplication as a cause of familial Parkinson's disease. *Lancet* **364**, 1167–1169 (2004).
23. A. B. Singleton, M. Farrer, J. Johnson, A. Singleton, S. Hague, J. Kachergus, M. Hulihan, T. Peuralinna, A. Dutra, R. Nussbaum, S. Lincoln, A. Crawley, M. Hanson, D. Maraganore, C. Adler, M. R. Cookson, M. Muenter, M. Baptista, D. Miller, J. Blancato, J. Hardy, K. Gwinn-Hardy, α-Synuclein locus triplication causes Parkinson's disease. *Science* **302**, 841 (2003).
24. N. P. Visanji, J. M. Brotchie, L. V. Kalia, J. B. Koprich, A. Tandon, J. C. Watts, A. E. Lang, α-Synuclein-based animal models of Parkinson's disease: Challenges and opportunities in a new era. *Trends Neurosci.* **39**, 750–762 (2016).
25. D. Kirik, C. Rosenblad, C. Burger, C. Lundberg, T. E. Johansen, N. Muzyczka, R. J. Mandel, A. Björklund, Parkinson-like neurodegeneration induced by targeted overexpression of α-synuclein in the nigrostriatal system. *J. Neurosci.* **22**, 2780–2791 (2002).
26. N. Zhao, C.-C. Liu, A. J. van Ingelgom, C. Linares, A. Kurti, J. A. Knight, M. G. Heckman, N. N. Diehl, M. Shinohara, Y. A. Martens, O. N. Attrebi, L. Petrucelli, J. D. Fryer, Z. K. Wszolek, N. R. Graff-Radford, R. J. Caselli, M. Y. Sanchez-Contreras, R. Rademakers, M. E. Murray, S. Koga, D. W. Dickson, O. A. Ross, G. Bu, APOE ε2 is associated with increased tau pathology in primary tauopathy. *Nat. Commun.* **9**, 4388 (2018).
27. M. Delenclos, A. H. Faroqi, M. Yue, A. Kurti, M. Castanedes-Casey, L. Rousseau, V. Phillips, D. W. Dickson, J. D. Fryer, P. J. McLean, Neonatal AAV delivery of alpha-synuclein induces pathology in the adult mouse brain. *Acta Neuropathol. Commun.* **5**, 51 (2017).
28. P. M. Sullivan, B. Han, F. Liu, B. E. Mace, J. F. Ervin, S. Wu, D. Koger, S. Paul, K. R. Bales, Reduced levels of human apoE4 protein in an animal model of cognitive impairment. *Neurobiol. Aging* **32**, 791–801 (2011).

29. G. G. Kovacs, L. Breydo, R. Green, V. Kis, G. Puska, P. Lőrincz, L. Perju-Dumbrava, R. Giera, W. Pirker, M. Lutz, I. Lachmann, H. Budka, V. N. Uversky, K. Molnár, L. László, Intracellular processing of disease-associated α-synuclein in the human brain suggests prion-like cell-to-cell spread. *Neurobiol. Dis.* **69**, 76–92 (2014).
30. G. G. Kovacs, U. Wagner, B. Dumont, M. Pikkarainen, A. A. Osman, N. Streichenberger, I. Leisser, J. Verchère, T. Baron, I. Alafuzoff, H. Budka, A. Perret-Liaudet, I. Lachmann, An antibody with high reactivity for disease-associated α-synuclein reveals extensive brain pathology. *Acta Neuropathol.* **124**, 37–50 (2012).
31. H. Fujiwara, M. Hasegawa, N. Dohmae, A. Kawashima, E. Masliah, M. S. Goldberg, J. Shen, K. Takio, T. Iwatsubo, α-synuclein is phosphorylated in synucleinopathy lesions. *Nat. Cell Biol.* **4**, 160–164 (2002).
32. I. Magen, M.-F. Chesselet, Mouse models of cognitive deficits due to alpha-synuclein pathology. *J. Park. Dis.* **1**, 217–227 (2011).
33. D. Aarsland, M. Beyer, M. Kurz, Dementia in Parkinson's disease. *Curr. Opin. Neurol.* **21**, 676–682 (2008).
34. D. J. Burn, Cortical Lewy body disease. *J. Neurol. Neurosurg. Psychiatry* **75**, 175–178 (2004).
35. K. Jellinger, Overview of morphological changes in Parkinson's disease. *Adv. Neurol.* **45**, 1–18 (1987).
36. M. R. Cookson, α-Synuclein and neuronal cell death. *Mol. Neurodegener.* **4**, 9 (2009).
37. A. N. Sacino, M. Brooks, A. B. McKinney, M. A. Thomas, G. Shaw, T. E. Golde, B. I. Giasson, Brain injection of α-synuclein induces multiple proteinopathies, gliosis, and a neuronal injury marker. *J. Neurosci.* **34**, 12368–12378 (2014).
38. J. E. Burda, M. V. Sofroniew, Reactive gliosis and the multicellular response to CNS damage and disease. *Neuron* **81**, 229–248 (2014).
39. D. W. Dickson, M. G. Heckman, M. E. Murray, A. I. Soto, R. L. Walton, N. N. Diehl, J. A. van Gerpen, R. J. Uitti, Z. K. Wszolek, N. Ertekin-Taner, D. S. Knopman, R. C. Petersen, N. R. Graff-Radford, B. F. Boeve, G. Bu, T. J. Ferman, O. A. Ross, APOEε4 is associated with severity of Lewy body pathology independent of Alzheimer pathology. *Neurology* **91**, e1182–e1195 (2018).
40. J. L. Robinson, E. B. Lee, S. X. Xie, L. Rennert, E. Suh, C. Bredenberg, C. Caswell, V. M. van Deerlin, N. Yan, A. Yousef, H. I. Hurtig, A. Siderowf, M. Grossman, C. T. McMillan, B. Miller, J. E. Duda, D. J. Irwin, D. Wolk, L. Elman, L. McCluskey, A. Chen-Plotkin, D. Weintraub, S. E. Arnold, J. Brettschneider, V. M. Y. Lee, J. Q. Trojanowski, Neurodegenerative disease concomitant proteinopathies are prevalent, age-related and APOE4-associated. *Brain* **141**, 2181–2193 (2018).
41. G. W. Beecham, K. Hamilton, A. C. Naj, E. R. Martin, M. Huentelman, A. J. Myers, J. J. Corneveaux, J. Hardy, J.-P. Vonsattel, S. G. Younkin, D. A. Bennett, P. L. de Jager, E. B. Larson, P. K. Crane, M. I. Kamboh, J. K. Kofler, D. C. Mash, L. Duque, J. R. Gilbert, H. Gwirtsman, J. D. Buxbaum, P. Kramer, D. W. Dickson, L. A. Farrer, M. P. Frosch, B. Ghetti, J. L. Haines, B. T. Hyman, W. A. Kukull, R. P. Mayeux, M. A. Pericak-Vance, J. A. Schneider, J. Q. Trojanowski, E. M. Reiman; Alzheimer's Disease Genetics Consortium (ADGC), G. D. Schellenberg, T. J. Montine, Genome-wide association meta-analysis of neuropathologic features of Alzheimer's disease and related dementias. *PLOS Genet.* **10**, e1004606 (2014).
42. T. F. Tropea, S. X. Xie, J. Rick, L. M. Chahine, N. Dahodwala, J. Doshi, C. Davatzikos, L. M. Shaw, V. van Deerlin, J. Q. Trojanowski, D. Weintraub, A. S. Chen-Plotkin, APOE, thought disorder, and SPARE-AD predict cognitive decline in established Parkinson's disease. *Mov. Disord.* **33**, 289–297 (2018).
43. H. Apaydin, J. E. Ahlskog, J. E. Parisi, B. F. Boeve, D. W. Dickson, Parkinson disease neuropathology: Later-developing dementia and loss of the levodopa response. *Arch. Neurol.* **59**, 102–112 (2002).
44. J. M. Olichney, D. Galasko, D. P. Salmon, C. R. Hofstetter, L. A. Hansen, R. Katzman, L. J. Thal, Cognitive decline is faster in Lewy body variant than in Alzheimer's disease. *Neurology* **51**, 351–357 (1998).
45. W. S. Davidson, A. Jonas, D. F. Clayton, J. M. George, Stabilization of α-synuclein secondary structure upon binding to synthetic membranes. *J. Biol. Chem.* **273**, 9443–9449 (1998).
46. S. Petrucci, M. Ginevrino, E. M. Valente, Phenotypic spectrum of alpha-synuclein mutations: New insights from patients and cellular models. *Parkinsonism Relat. Disord.* **22** (Suppl. 1), S16–S20 (2016).
47. D. Twohig, E. Rodriguez-Vieitez, S. B. Sando, G. Berge, C. Lauridsen, I. Møller, G. R. Grøntvedt, G. Bråthen, K. Patra, G. Bu, T. L. S. Benzinger, C. M. Karch, A. Fagan, J. C. Morris, R. J. Bateman, A. Nordberg, L. R. White, H. M. Nielsen; Dominantly Inherited Alzheimer Network (DIAN), The relevance of cerebrospinal fluid α-synuclein levels to sporadic and familial Alzheimer's disease. *Acta Neuropathol. Commun.* **6**, 130 (2018).
48. C. Galvagnion, The role of lipids interacting with α-synuclein in the pathogenesis of Parkinson's Disease. *J. Park. Dis.* **7**, 433–450 (2017).
49. R. W. Mahley, Apolipoprotein E: Cholesterol transport protein with expanding role in cell biology. *Science* **240**, 622–630 (1988).
50. M. Shinohara, T. Kanekiyo, L. Yang, D. Linthicum, M. Shinohara, Y. Fu, L. Price, J. L. Frisch-Daiello, X. Han, J. D. Fryer, G. Bu, APOE2 eases cognitive decline during Aging: Clinical and preclinical evaluations. *Ann. Neurol.* **79**, 758–774 (2016).
51. T. G. Beach, C. H. Adler, L. I. Sue, L. Vedders, L. Lue, C. L. White III, H. Akiyama, J. N. Caviness, H. A. Shill, M. N. Sabbagh, D. G. Walker; Arizona Parkinson's Disease Consortium, Multi-organ distribution of phosphorylated α-synuclein histopathology in subjects with Lewy body disorders. *Acta Neuropathol.* **119**, 689–702 (2010).
52. F. N. Emamzadeh, D. Allsop, α-synuclein interacts with lipoproteins in plasma. *J. Mol. Neurosci.* **63**, 165–172 (2017).
53. F. N. Emamzadeh, Role of apolipoproteins and α-synuclein in Parkinson's disease. *J. Mol. Neurosci.* **62**, 344–355 (2017).
54. F. N. Emamzadeh, H. Aojula, P. C. McHugh, D. Allsop, Effects of different isoforms of apoE on aggregation of the α-synuclein protein implicated in Parkinson's disease. *Neurosci. Lett.* **618**, 146–151 (2016).
55. H.-J. Lee, E.-J. Bae, S.-J. Lee, Extracellular α-synuclein—A novel and crucial factor in Lewy body diseases. *Nat. Rev. Neurol.* **10**, 92–98 (2014).
56. J. D. Ulrich, J. M. Burchett, J. L. Restivo, D. R. Schuler, P. B. Verghese, T. E. Mahan, G. E. Landreth, J. M. Castellano, H. Jiang, J. R. Cirrito, D. M. Holtzman, In vivo measurement of apolipoprotein E from the brain interstitial fluid using microdialysis. *Mol. Neurodegener.* **8**, 13 (2013).
57. T. M. Achariyar, B. Li, W. Peng, P. B. Verghese, Y. Shi, E. McConnell, A. Benraiss, T. Kasper, W. Song, T. Takano, D. M. Holtzman, M. Nedergaard, R. Deane, Glymphatic distribution of CSF-derived apoE into brain is isoform specific and suppressed during sleep deprivation. *Mol. Neurodegener.* **11**, 74 (2016).
58. P. Dzeja, A. Terzic, Adenylate kinase and AMP signaling networks: Metabolic monitoring, signal communication and body energy sensing. *Int. J. Mol. Sci.* **10**, 1729–1772 (2009).
59. A. Fernandez-Gonzalez, S. Kourembanas, T. A. Wyatt, S. A. Mitsialis, Mutation of murine adenylate kinase 7 underlies a primary ciliary dyskinesia phenotype. *Am. J. Respir. Cell Mol. Biol.* **40**, 305–313 (2009).
60. Y. Miyamoto, N. Kitamura, Y. Nakamura, M. Futamura, T. Miyamoto, M. Yoshida, M. Ono, S. Ichinose, H. Arakawa, Possible existence of lysosome-like organella within mitochondria and its role in mitochondrial quality control. *PLOS ONE* **6**, e16054 (2011).
61. N. Kitamura, Y. Nakamura, Y. Miyamoto, T. Miyamoto, K. Kabu, M. Yoshida, M. Futamura, S. Ichinose, H. Arakawa, Mieap, a p53-inducible protein, controls mitochondrial quality by repairing or eliminating unhealthy mitochondria. *PLOS ONE* **6**, e16060 (2011).
62. Y. Nakamura, N. Kitamura, D. Shinogi, M. Yoshida, O. Goda, R. Murai, H. Kamino, H. Arakawa, BNIP3 and NIX mediate Mieap-induced accumulation of lysosomal proteins within mitochondria. *PLOS ONE* **7**, e30767 (2012).
63. R. Roesler, G. Schwartsmann, Gastrin-releasing peptide receptors in the central nervous system: Role in brain function and as a drug target. *Front. Endocrinol.* **3**, 159 (2012).
64. Y. Shi, K. Yamada, S. A. Liddelow, S. T. Smith, L. Zhao, W. Luo, R. M. Tsai, S. Spina, L. T. Grinberg, J. C. Rojas, G. Gallardo, K. Wang, J. Roh, G. Robinson, M. B. Finn, H. Jiang, P. M. Sullivan, C. Baufeld, M. W. Wood, C. Sutphen, L. McCue, C. Xiong, J. L. Del-Aguila, J. C. Morris, C. Cruchaga; Alzheimer's Disease Neuroimaging Initiative, A. M. Fagan, B. L. Miller, A. L. Boxer, W. W. Seeley, O. Butovsky, B. A. Barres, S. M. Paul, D. M. Holtzman, ApoE4 markedly exacerbates tau-mediated neurodegeneration in a mouse model of tauopathy. *Nature* **549**, 523–527 (2017).
65. A. M. Wennberg, N. Tosakulwong, T. G. Lesnick, M. E. Murray, J. L. Whitwell, A. M. Liesinger, L. Petrucelli, B. F. Boeve, J. E. Parisi, D. S. Knopman, R. C. Petersen, D. W. Dickson, K. A. Josephs, Association of apolipoprotein E ε4 with transactive response DNA-binding protein 43. *JAMA Neurol.* **75**, 1347–1354 (2018).
66. H.-S. Yang, L. Yu, C. C. White, L. B. Chibnik, J. P. Chhatwal, R. A. Sperling, D. A. Bennett, J. A. Schneider, P. L. De Jager, Evaluation of TDP-43 proteinopathy and hippocampal sclerosis in relation to APOE ε4 haplotype status: A community-based cohort study. *Lancet Neurol.* **17**, 773–781 (2018).
67. C. Koriath, T. Lashley, W. Taylor, R. Druyeh, A. Dimitriadis, N. Denning, J. Williams, J. D. Warren, N. C. Fox, J. M. Schott, J. B. Rowe, J. Collinge, J. D. Rohrer, S. Mead, ApoE4 lowers age at onset in patients with frontotemporal dementia and tauopathy independent of amyloid-β copathology. *Alzheimers Dement.* **11**, 277–280 (2019).
68. D. W. Dickson, M. L. Schmidt, V. M.-Y. Lee, M. L. Zhao, S.-H. Yen, J. Q. Trojanowski, Immunoreactivity profile of hippocampal CA2/3 neurites in diffuse Lewy body disease. *Acta Neuropathol.* **87**, 269–276 (1994).
69. D. H. Adamowicz, S. Roy, D. P. Salmon, D. R. Galasko, L. A. Hansen, E. Masliah, F. H. Gage, Hippocampal α-synuclein in dementia with lewy bodies contributes to memory impairment and is consistent with spread of pathology. *J. Neurosci.* **37**, 1675–1684 (2017).
70. M. Riekkinen, K. Kejonen, P. Jäkälä, H. Soininen, P. Riekkinen Jr., Reduction of noradrenaline impairs attention and dopamine depletion slows responses in Parkinson's disease. *Eur. J. Neurosci.* **10**, 1429–1435 (1998).
71. N. Sawamoto, P. Piccini, G. Hotton, N. Pavese, K. Thielemans, D. J. Brooks, Cognitive deficits and striato-frontal dopamine release in Parkinson's disease. *Brain* **131**, 1294–1302 (2008).
72. G. M. Halliday, J. B. Leverenz, J. S. Schneider, C. H. Adler, The neurobiological basis of cognitive impairment in Parkinson's disease. *Mov. Disord.* **29**, 634–650 (2014).
73. C.-C. Liu, C.-W. Tsai, F. Deak, J. Rogers, M. Penuliar, Y. M. Sung, J. N. Maher, Y. Fu, X. Li, H. Xu, S. Estus, H.-S. Hoe, J. D. Fryer, T. Kanekiyo, G. Bu, Deficiency in LRP6-mediated Wnt

signaling contributes to synaptic abnormalities and amyloid pathology in Alzheimer's disease. *Neuron* **84**, 63–77 (2014).
74. C.-C. Liu, N. Zhao, Y. Yamaguchi, J. R. Cirrito, T. Kanekiyo, D. M. Holtzman, G. Bu, Neuronal heparan sulfates promote amyloid pathology by modulating brain amyloid-beta clearance and aggregation in Alzheimer's disease. *Sci. Transl. Med.* **8**, 332ra44 (2016).
75. M. Shinohara, M. E. Murray, R. D. Frank, M. Shinohara, M. DeTure, Y. Yamazaki, M. Tachibana, Y. Atagi, M. D. Davis, C.-C. Liu, N. Zhao, M. M. Painter, R. C. Petersen, J. D. Fryer, J. E. Crook, D. W. Dickson, G. Bu, T. Kanekiyo, Impact of sex and APOE4 on cerebral amyloid angiopathy in Alzheimer's disease. *Acta Neuropathol.* **132**, 225–234 (2016).
76. N. Zhao, C.-C. Liu, A. J. van Ingelgom, Y. A. Martens, C. Linares, J. A. Knight, M. M. Painter, P. M. Sullivan, G. Bu, Apolipoprotein E4 impairs neuronal insulin signaling by trapping insulin receptor in the endosomes. *Neuron* **96**, 115–129.e5 (2017).
77. Q. Liu, J. Trotter, J. Zhang, M. M. Peters, H. Cheng, J. Bao, X. Han, E. J. Weeber, G. Bu, Neuronal LRP1 knockout in adult mice leads to impaired brain lipid metabolism and progressive, age-dependent synapse loss and neurodegeneration. *J. Neurosci.* **30**, 17068–17078 (2010).
78. T. Maejima, P. Wollenweber, L. U. C. Teusner, J. L. Noebels, S. Herlitze, M. D. Mark, Postnatal loss of P/Q-type channels confined to rhombic-lip-derived neurons alters synaptic transmission at the parallel fiber to purkinje cell synapse and replicates genomic Cacna1a mutation phenotype of ataxia and seizures in mice. *J. Neurosci.* **33**, 5162–5174 (2013).
79. S. J. Guyenet, S. A. Furrer, V. M. Damian, T. D. Baughan, A. R. La Spada, G. A. Garden, A simple composite phenotype scoring system for evaluating mouse models of cerebellar ataxia. *J. Vis. Exp.* , 1787 (2010).
80. J.-W. Zhu, Y.-F. Li, Z.-T. Wang, W.-Q. Jia, R.-X. Xu, Toll-like receptor 4 deficiency impairs motor coordination. *Front. Neurosci.* **10**, 33 (2016).
81. K. R. Kalari, A. A. Nair, J. D. Bhavsar, D. R. O'Brien, J. I. Davila, M. A. Bockol, J. Nie, X. Tang, S. Baheti, J. B. Doughty, S. Middha, H. Sicotte, A. E. Thompson, Y. W. Asmann, J.-P. A. Kocher, MAP-RSeq: Mayo analysis pipeline for RNA sequencing. *BMC Bioinformatics* **15**, 224 (2014).
82. K. D. Hansen, R. A. Irizarry, Z. Wu, Removing technical variability in RNA-seq data using conditional quantile normalization. *Biostatistics* **13**, 204–216 (2012).
83. P. Langfelder, S. Horvath, WGCNA: An R package for weighted correlation network analysis. *BMC Bioinformatics* **9**, 559 (2008).
84. Z. Hu, Y.-C. Chang, Y. Wang, C.-L. Huang, Y. Liu, F. Tian, B. Granger, C. DeLisi, VisANT 4.0: Integrative network platform to connect genes, drugs, diseases and therapies. *Nucleic Acids Res.* **41**, W225–W231 (2013).

Acknowledgments: We thank P. M. Sullivan (Duke University Medical Center, Durham, NC) for developing and contributing the APOE-TR mice and K. Jansen-West and E. A. Perkerson for preparing AAV–α-synuclein and AAV-GFP viruses. We are grateful to V. Phillips and M. Castanedes-Casey for histologic and immunohistochemical support. We thank S. Koga for assisting with Aperio ImageScope training for image analysis studies. **Funding:** This work was supported by NIH grants R37AG027924, RF1AG057181, R01AG035355, RF1AG046205, RF1AG051504, and P01NS074969 to G.B. and Lewy Body Dementia Center Without Walls U54NS110435 to D.W.D., P.J.M., O.A.R., J.D.F., C.-C.L., N.Z., and G.B. The brain bank was supported, in part, by the Mangurian Foundation Lewy Body Dementia Program at Mayo Clinic. **Author contributions:** N.Z. and G.B. developed the research concept and designed the experiments; N.Z. and O.N.A. performed all the animal experiments; Y.R., W.Q., and Y.W.A. performed bioinformatics analysis of the RNA-seq data; B.S. and A.D.M. worked on IHC scanning and quantification blindly; F.L. worked on Western blotting; W.Q. and Y.A.M. helped with mouse brain lysate preparation and RNA preparation; F.S. worked with α-synuclein ELISA detection; J.Z. performed the qPCR; A.J.V.I. helped with the mouse breeding setup and maintenance; M.D.D. and C.-C.L. helped with the viral preparation; A.K. did the mouse behavioral tests; J.A.K., C.L., and Y.C. contributed to the animal maintenance and brain tissue preparation; M.D. helped with immunostaining and biochemical analysis setup; P.J.M. provided AAV–α-synuclein and AAV-GFP viruses; J.D.F. supported the animal behavioral tests; D.W.D. provided the human postmortem brain samples; N.Z., D.W.D., O.A.R., and G.B. wrote the manuscript with critical inputs and edits by the coauthors. **Competing interests:** The authors declare that they have no competing interests. **Data and materials availability:** All the data used for this study are present in the paper or the Supplementary Materials.

Submitted 6 June 2019
Accepted 3 December 2019
Published 5 February 2020
10.1126/scitranslmed.aay1809

Citation: N. Zhao, O. N. Attrebi, Y. Ren, W. Qiao, B. Sonustun, Y. A. Martens, A. D. Meneses, F. Li, F. Shue, J. Zheng, A. J. Van Ingelgom, M. D. Davis, A. Kurti, J. A. Knight, C. Linares, Y. Chen, M. Delenclos, C.-C. Liu, J. D. Fryer, Y. W. Asmann, P. J. McLean, D. W. Dickson, O. A. Ross, G. Bu, APOE4 exacerbates α-synuclein pathology and related toxicity independent of amyloid. *Sci. Transl. Med.* **12**, eaay1809 (2020).

Science Translational Medicine

APOE4 exacerbates α-synuclein pathology and related toxicity independent of amyloid

Na Zhao, Olivia N. Attrebi, Yingxue Ren, Wenhui Qiao, Berkiye Sonustun, Yuka A. Martens, Axel D. Meneses, Fuyao Li, Francis Shue, Jiaying Zheng, Alexandra J. Van Ingelgom, Mary D. Davis, Aishe Kurti, Joshua A. Knight, Cynthia Linares, Yixing Chen, Marion Delenclos, Chia-Chen Liu, John D. Fryer, Yan W. Asmann, Pamela J. McLean, Dennis W. Dickson, Owen A. Ross and Guojun Bu

Sci Transl Med **12**, eaay1809.
DOI: 10.1126/scitranslmed.aay1809

APOE4 beyond amyloid

Although several genetic risk factors for neurodegenerative disorders have been identified, often the mechanistic aspect is not clear. Now, Zhao *et al.* and Davis *et al.* investigated whether apolipoprotein E4 (APOE4) genotype, a major genetic risk factor for neurodegenerative diseases, affected α-synuclein pathology in mouse models and Parkinson's disease (PD) patients. Zhao *et al.* generated a mouse model of α-synucleinopathy and showed that APOE4 exacerbated α-synuclein pathology in the absence of amyloid. Davis *et al.* used a mouse model of PD and analyzed cognition in patients with PD to demonstrate that APOE4 directly regulated α-synuclein pathology and was associated with faster cognitive decline. These results provide insight into the mechanisms linking APOE genotype to neurodegenerative disorders.